FINAL REPORT HH 01/15

EuroPoint- Investigating the heating of electrically heated points in railway construction

Customer	SBB AG
	Kompetenzzentrum Weichenheizung
	Zentralstrasse 1
	6003 Luzern
	Schweiz
Contractor	Technische Universität Dresden
	Institute of Electrical Power Systems and High Voltage Engineering Chair of High Voltage and High Current Engineering 01062 Dresden
Order	contract from 29.10.2015, order no. 4700240630 from 19.04.2016
Project period	14.12.2015 to 31.12.2019
Data of report	03.03.2020
Scope of report	61 pages, 15 Attachments
Responsible at customer	Daniel Föhn
Responsible at contractor	Markus Schladitz
checked	Robert Adam
confirmed	Prof. Dr.-Ing. Steffen Großmann
Copy to	1 x Customer (English; printed and electronic document (PDF))
	1 x Customer (German; printed and electronic document (PDF))
	1 x Institute
	1 x Contractor - Person in charge

Contents

1 Introduction

The points of railroad facilities have to be heated to ensure the operational reliability of railway tracks and station rails and to enable a safe and punctual train operation. For this purpose, many different kinds of point heaters have been developed at the railway companies during the marge of time. They differ in the used energy source (electrical energy, gas or geothermal), the construction of the heating elements, the kind of installation at the track as well as in the close and open loop control of the point heating systems. Because of the big amount of points in railroad facilities, the applied energy is very high for point heating and thus represents a significant cost factor for the operation. The knowledge about the required amount of heat, its time response and its spatial allocation is less available at the manufacturer and operating companies. It is usually generated empirically. Statements on the reliability of the point heating systems influenced by ambient conditions cannot be made until now. To be able to evaluate the efficiency and the effectivity it is necessary to develop a thermal model, which

- can compute the temperature rise of a heated point systems,
- can help to understand the processes of heat generation, heat loss, heat transfer and heat transport,
- can illustrate the heat flows quantitatively
- and can display the temperature distribution of the point system.

By systematic researches of the thermal conditions of point heaters and by using the knowledge about it for designing the components as well as their operation the amount of energy that is used is to be reduced and the functional reliability is to be increased. For this purpose, the processes of heat generation, heat storage and heat transport have to be described. Point heaters are equipment for outdoor conditions. The parameters of heat transmission and heat storage are unknown in connection with the application of heating calculation for railway constructions so far. The processes of heat transmission and heat storage have to be researched for the usage of thermal models when calculating the heating of point systems.

The common motivation of several European railway companies is the effort to be able to estimate the efficiency and the effectivity of point heaters, to optimize the use of energy and to increase the functional reliability. On this basis the European railway companies (SNCF, ÖBB, SBB, Infrabel und ProRail), the Institut für Verkehrsinfrastruktur (i-vis) und the Institut für Elektrische Energieversorgung und Hochspannungstechnik (IEEH) of the TU DRESDEN have banded together to the research cooperation called "EuroPoint / Euroweiche". It is the aim of the research cooperation to develop a common thermal model of a point "EuroPoint" in form of a thermal network. The thermal network of the EuroPoint is to serve as the basic tool and reference model for thermal calculation of point systems.

2 Definition of the project object „EuroPoint"

Different kinds of technical solutions have been evolved by the European railway companies for the construction of railway tracks during marge of time. This means a high diversity of systems for heating the points (**Figure 1**).
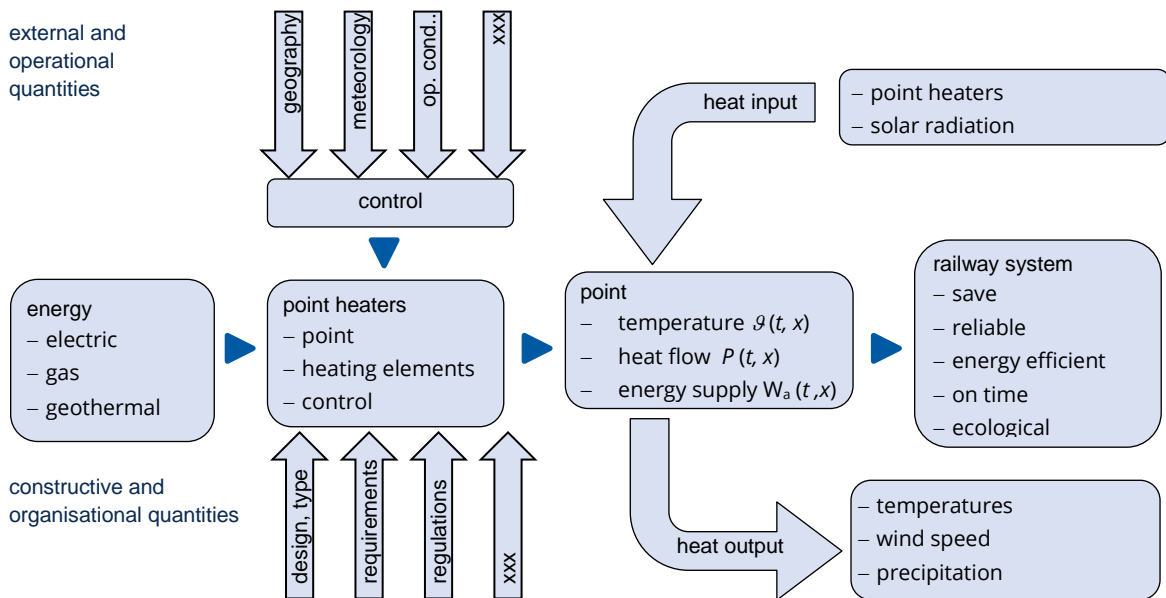

Figure 1: the system of point heating and its influencing variables

Because of the construction of the points, the various point heating systems differ. Different rail profiles, sleepers and track beds are combined together in alternating ways. The heating elements itself and their mounting must be adapted to the given construction of the point. Electricity, gas or geothermal energy are available as energy sources. The requirements to the operation of the heating systems are determined differently by the companies depending on the external influencing variables and the desired operating. This results in different control and regulation for the operation of the point heaters. The basic processes of heating as well as the distribution of heat flow rates and temperatures can be described by thermal models despite the big diversity that point heating system have. This can be simulated by thermal networks for example. It is necessary to develop one common model of a heated point system, called the EuroPoint, out of the huge amount of different constructions. Such a common model has to comply several requirements. It should represent an as large as possible number of point that are used at the line network of the participating railway companies. It is advantageously for the experimental researches, to choose a combination of single components that are really built that way in the line network. The point heating itself should represent a standard solution that is used by any railway company.

2.1   Terms and definitions for the thermal model

At first, some of the terms are to be explained concerning the points, to facilitate the communication between the participating railway companies the IEEH and i-vis. In this case, the component should be taken into account that are necessary for calculating the heating of points.

Initially, the generally geometrical parameters are necessary for the heating of a point. The geometry is defined dominantly by the type of point (e. g. standard right- or left-hand switch, double-slip switch), the used rail profile (e. g. UIC 60, S 49) (**Figure 2**).
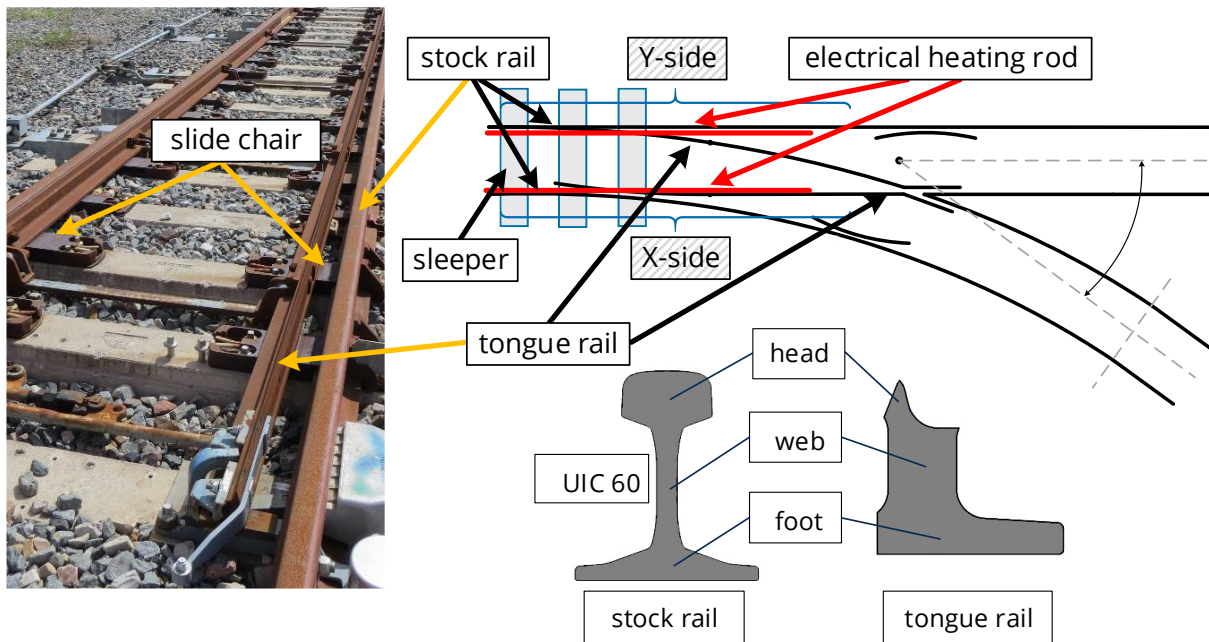

Figure 2: terms of the point system

The length of a point is rated by the radius R of the branching track and by the frog angle α. This takes into account the general parameters of the geometry.

Heat transmission occurs by the physical effects of the heat conduction the heat radiation and the heat convection. The cross section areas and the material properties of thermal conductivity λ have to be known for describing the heat conduction within the components of a point. The cross section area of the stock rail and the tongue rail for conducting heat are determined by the rail profile (e. g. UIC 60) and by the kind of tongue rail (e. g. flexible switch) that is used. Heat can be transported between the stock and the tongue rail by heat conduction through the installed slide chairs and by radiation of the opposite surfaces. The size and arrangement of the surfaces involved are decisive for heat radiation.

The heat conduction from the rails into the track bed occurs by the slide chairs and the sleepers (e. g. steel, concrete). It is essential how the slide chairs are mounted on the sleepers (bracing between stock rail and slide chair, fastening of the slide chair on the base plate and the sleeper). The geometry, the material and the positioning along the

point are decisive for the heat flow into the track bed. Furthermore, heat can be conducted through the used point lock system on one hand between the stock and the tongue rails of both sides of the track and on the other hand into the track bed. The contact that is determining the heat conduction between the tongue rail and the slide chair can be influenced by the tongue rail itself and by the use of rolling systems.

Thermal power has to be applied into the system to rise the temperature of the point. It is decisive what kind of heating element are used (e. g. electric heat rod, gas burner). For this, the heat output, the geometry and the position of the heating elements are especially important. The contact between the electric heating elements and the rails are determined by the type of installation. The choice of the used mounting elements (e. g. clamps) and their distribution along the heating elements is crucial at that point. The thermal capacities of all components have to be considered in order to be able to calculate the time dependent temperature distribution at the point. For this, the material properties of the specific heat c_s and the density δ as well as the volume are needed. This can be determined by the general geometric parameters of the components.

2.2 Selection of the components for the EuroPoint

Each of the railway companies participating in the project uses different products and types for the. The model of the Euroweiche / EuroPoint represents a mutual combination of these components. A proposal of a common configuration is deduced from a survey to the participating railway companies. In mutual agreement, the models for the components were selected which on the one hand are frequently used and on the other hand can be made available by the railway companies for experimental investigations (**Table 1**).

Table 1: assignment of the models for the components of the EuroPoint

component	model
stock rail	rail profile UIC 60
tongue rail	flexible switch profile UIC 60
base plate	combined component RPG50-60
slide chair	
sleeper	WS:601200 KOMPL

In Europe, standards have been developed for the used rails. The UIC 60 profile is the most common rail profile and shall be use for the EuroPoint (**Figure 3**). The tongue rail shall be performed as a flexible switch.
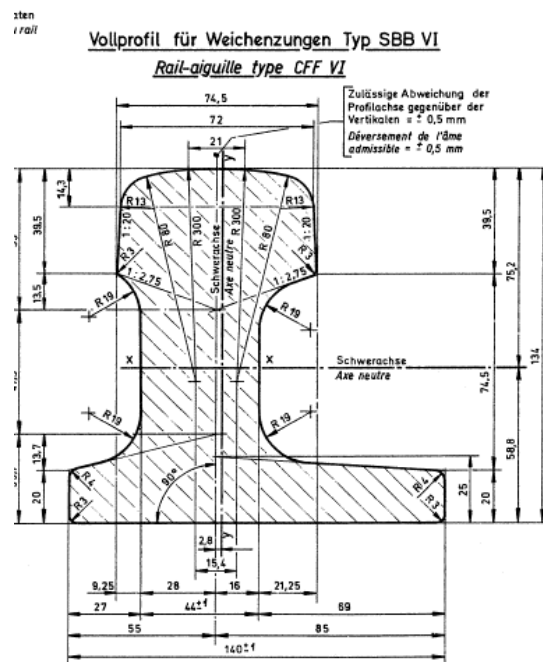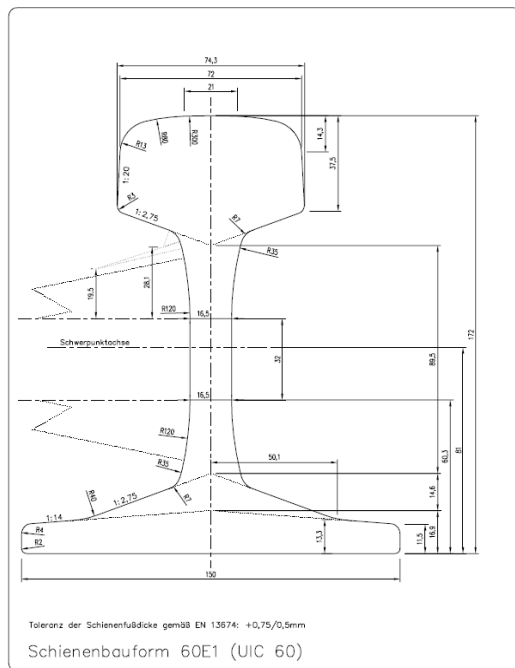
Figure 3: rail profile UIC 60 for stock and tongue rail

The stock rail and tongue rail are mounted together on the slide chairs. The stock rail is firmly clamped to the slide chair. The movement of the tongue rail is ensured either by slide plates or by roller devices integrated in the slide plates. Slide chairs with integrated rolls have so far only been used to a limited extent in the rail networks of European railway companies. A simple slide chair with slide plates (SCHWIHAG BGL 606) and internal stock rail tensioning (IBAV) is therefore selected for the EuroPoint model.

The majority of the sleepers used today are made of concrete. The centre distance of the single sleepers is 600 mm. Point locks are used to lock the tongue rail in its end position. A commonly used type is the clamp lock. A clamp lock of the type WKV 50-2 (BHARAT FORGE CDP GmbH) is selected for the model of the EuroPoint. Electric heating elements are one of the most common ways to feed heating power into the points. Therefore, RKW heating elements (TÜRK + HILLINGER GmbH) are to be used as the heat source for the EuroPoint. The heating rods are to be mounted on the rails of the point with the corresponding fixtures for the connecting head and clamping brackets of the same manufacturer (**Figure 4**). A clamp-to-clamp distance of 30 cm will be used for fixing.
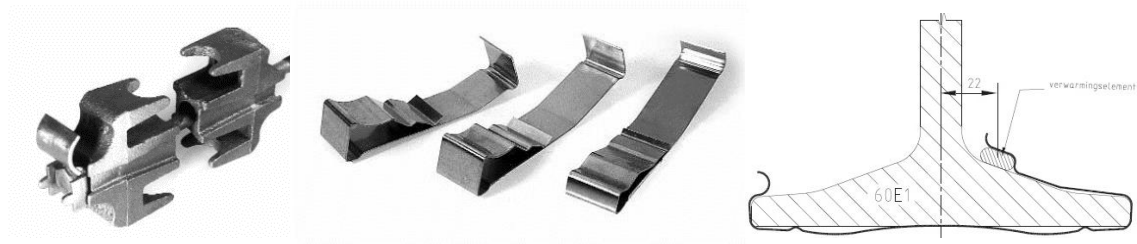
Figure 4: fastening clamps and mounting position of the heating rod

2.3 Application conditions for point heating

Most point heating systems today are operated remotely by means of automatic control. The criteria for switching on and off are the air temperature and the occurrence of precipitation. The thermal model (heating network) of the EuroPoint is used to check whether and to what extent the requirements defined by the railways for a heating system can be met. In addition to these two control parameters, other environmental conditions must also be considered. These include wind speed, wind direction and global radiation. Implementation possibilities for these parameters must be found in the thermal model. Both the thermal effect of the environmental conditions separately from each other and in combination is of great interest for the calculation of the heating. Precipitation can occur in the form of rain or snowfall. For both types there is still no experience regarding the consideration in the heat network. Therefore, it is important that the theoretical findings are supported by practical investigations.

3 Heating calculations with thermal networks

In addition to the thermal network method, a calculation with FEM models is also possible, which is often used for heating calculations. However, a calculation using the thermal network is advantageous for calculating the heating of a point, as individual subnetworks can be linked to each other without problems. Furthermore, the calculation time is relatively short and thus parameter studies can be carried out effectively.

When the physical quantities of the electric field and of the thermal field are compared, a clear analogy can be observed (**Table 2**). The flow quantity is known as the current I in the electric field. In the thermal field, this corresponds to the heat flow P.

Table 2:   quantities of the electric and the thermic field

quantity	electric	thermic
current / flow	I	P
potential difference	$\Delta\varphi = U = I \cdot R_{el}$	$\Delta\vartheta = P \cdot R_{th}$
resistance	$R_{el} = l \cdot \kappa^{-1} A^{-1}$	$R_{th} = l \cdot \lambda^{-1} A^{-1}$
capacity	$C_{el} = \varepsilon \cdot A \cdot l^{-1}$	$C_{th} = c \cdot \delta \cdot V$
time constant	$\tau_{el} = C_{el}\cdot R_{el}$	$\tau_{th} = C_{th}\cdot R_{th}$

The potential difference of the electric field is the voltage U. The potential difference of the thermal field is the temperature difference $\Delta\vartheta$. It can be assumed that the processes of heat transfer can be described with similar methods like the electric transmission. This is called the thermal network method. In a thermal network, the heat transmission processes are simulated by heat sources, temperature sources, thermal resistors and thermal capacitors [1]. The method has already been used successfully for the calculation of the heating of electrical installations and devices of the power engineering. A summary of the physical quantities of heating can be found at [1][2].

Thermal power is emitted from the heat sources (e. g. heaters) to the heat sinks (e. g. environment) by heat conduction, heat radiation and convection. At thermal networks, the processes of heat transmission are symbolized by resistances. Similar to an electric network the transmitted heat flow $P(\vartheta)$ results from the quotient of the temperature difference $\Delta\vartheta$ and the thermal resistance $R_{th}(\vartheta)$.

$$P(\vartheta) = \frac{\Delta\vartheta}{R_{th}} \tag{1}$$

The thermal power $P_c(\vartheta)$ transmitted by conduction depends on the thermal conductivity λ of the media, the cross section area A which the heat flow passes through in normal direction and the gradient of the temperature grad ϑ.

$$P_c(\vartheta) = -\lambda \, A \, \mathrm{grad}\,\vartheta \tag{2}$$

The heat conduction resistance required for the thermal network is calculated from the geometry of the arrangement and the thermal conductivity. Thus, the heat conduction resistance for a rectangular body arises from the thermal conductivity $\lambda(\vartheta)$, that can be temperature depending, the distance d in direction of the heat flow as well as the height h and the width b of the vertical area.

$$R_C(\vartheta) = \frac{d}{\lambda(\vartheta)\,h\,b} \tag{3}$$

In order to calculate the heat conduction resistors, the cross-sectional areas available for heat conduction must therefore be determined. The heating power that is transmitted by heat radiation and convection is dependent on the heat transfer coefficient $\alpha(\vartheta)$, the surface O of the heat emitting body and the temperature difference $\Delta\vartheta$.

$$P(\vartheta) = \alpha(\vartheta)\,O\,\Delta\vartheta \tag{4}$$

If we compare this relationship with **eq. (1)**, this results in the general resistance to the heat transfer by radiation and convection.

$$R(\vartheta) = \frac{1}{\alpha(\vartheta)\,O} \tag{5}$$

All parameters of the corresponding heat transfer are summarized by the heat transfer coefficient $\alpha(\vartheta)$. The physical processes of the convective heat transfer are described by the similarity theory. With the resulting similarity criteria, the convective heat transfer coefficient $\alpha_{co}(\vartheta)$ can be described by the NUSSELT number Nu the conductivity λ_{med} of the fluid and the geometric magnitude of the characteristic length l_w.

$$\alpha_{co}(\vartheta) = Nu\,\frac{\lambda_{med}}{l_w} \tag{6}$$

The Nusselt number is calculated from the product of the Grashof number and the Prandtl number and the corresponding similarity parameters c_1 and n_1 (**eq (7)**).

$$Nu = c_1 \cdot (Gr \cdot Pr)^{n_1} \tag{7}$$

This equation of the Nusselt number applies to arrangements with free convection, i.e. the drive of the convection medium alone is a density difference. If the convection medium is additionally set in motion by fans or pumps, a forced convection occurs which superimposes the free convection. In this case, other similarity parameters must be used (**eq.(8)**).

$$Nu = c_2 \cdot Re^{\prime n_2} \tag{8}$$

The similarity criteria contained in the NUSSELT number (*Nu*) were determined experimentally for a large number of technical arrangements and can be found in literature **[1] [2]**. If we apply **eq. (1)** and **eq. (4)** only for the heat transfer by convection, the heat transfer resistance of the convection is obtained.

$$R_{co}(\vartheta) = \frac{1}{\alpha_{co}(\vartheta) O_{co}} \tag{9}$$

In order to be able to determine the heat transfer resistances of the convection, the similarity criteria and surfaces decisive for the heat transfer are required.

The heating power $P_r(\vartheta)$ that is transmitted by heat radiation is described by the STEFAN-BOLZMANN law. It depends on the absolute temperature *T* of the radiation exchanging bodies.

$$P_r = \varepsilon_{12}\, \sigma_r\, O_r \left[T_1^4 - T_2^4 \right] \tag{10}$$

If the general heat transfer equation (**eq. (4)**) is related only to the radiation component and equated with STEFAN-BOLTZMANN's law, the heat transfer coefficient of thermal radiation $\alpha_k(\vartheta)$ is obtained.

$$\alpha_r(\vartheta) = \frac{\varepsilon_{12}\, \sigma_r \left[T_1^4 - T_2^4 \right]}{\Delta \vartheta_{12}} \tag{11}$$

For calculating the heat transfer coefficient $\alpha_r(\vartheta)$ of the radiation the resulting emissivity ε_{12}, the STEFAN-BOLTZMANN constant σ_r, the absolute temperatures T_1 and T_2 and the temperature difference $\Delta \vartheta_{12}$ of the bodies involved in the radiation exchange are needed. The resulting emissivity ε_{12} arises from the ration of the surfaces O_1 and O_2 as well as the emissivities ε_1 and $_2$ of the two bodies.

$$\varepsilon_{12} = \frac{1}{\dfrac{1}{\varepsilon_1} + \dfrac{O_1}{O_2} \left(\dfrac{1}{\varepsilon_2} - 1 \right)} \tag{12}$$

The emissivity ε indicates the radiation ability of a real surface area in proportion to the radiation ability of the ideal black body. It depends on the material and on the surface conditions. The emissivity of several materials can be found in literature [**1**] and or can be

determined by measurements by a pyrometer. The heat resistance of the radiation is equivalent to that in **eq. (9)**.

$$R_r(\vartheta) = \frac{1}{\alpha_r(\vartheta)O_r}$$ (13)

$$P_r = F_{12} \cdot P_{r,sum}$$ (14)

The determination of the heat transfer resistances of the thermal radiation was thus carried out in the determination of the surfaces decisive for the thermal radiation and their radiant power.

The heat capacity of a body is the measure of how well it can store thermal energy. The greater the heat capacity, the more time a body needs for a defined temperature change with the same input thermal power (**eq. (15)**).

$$\Delta\vartheta = \frac{P \cdot t}{V \cdot \delta \cdot c_p}$$ (15)

c_p is the specific heat capacity, δ the density of the material and V the volume of the body. The heat capacity is needed to calculate the time-dependent heating of a body. The heat capacities are implemented in the heat network between the thermal nodes and zero potential.

A summary of the thermal quantities with the corresponding units can be found in **Attachment 1**. The heat network model is built with the program "Orcad Capture CIS".

4 Set up of the individual thermal networks

The thermal networks of the main components must be built up separately from each other and verified with a respective heating test. Only if the individual networks calculate the heating of the components correctly, it is possible to link them and thus to calculate the heating of the entire point correctly. The procedure for building the individual thermal networks is as follows:

- approximation of the geometry of the components
- thermal replication of the approximated geometry with resistors for thermal conduction
- implementation of resistors for convection and radiation at the interface to the ambience

- carrying out a heating test under laboratory conditions

- comparison of calculated and measured temperatures → adjustment of single thermal parameters

4.1 Set up of the thermal network of a stock rail with heating rod

Thermal conduction resistors for cuboid geometries with rectangular base areas are used for the construction. This means that the original UIC 60geometry of a stock rail cross section must first be approximated (**Figure 5**). The aim of the approximation is to convert the complex UIC 60 geometry into simple geometric shapes. However, there must be no significant differences in the size of volume and surface between the original and approximated geometry. A change of the volume influences the internal heat conduction and the heat storage of the stock rail. On the other hand, the size of the surface has an effect on the heat emitting processes convection and radiation (**eq. (5)**). Consequently, the surface area and circumference of both geometries were compared in the cross section (**Table 3**).

Figure 5: original and approximated geometry of a UIC 60 cross section of a stock rail

Table 3: comparison of original and approximated geometry of a stock rail

	original geometry	approximated geometry	ratio
area	7617 mm²	7718 mm²	1.013
circumference	678 mm	746 mm	1.100

The geometric differences are small and therefore the approximated geometry can be used to build up the thermal network of the stock rail. A decisive criterion for the accuracy with which a thermal network calculates temperatures is the network resolution. The higher the number of thermal nodes, the higher the temperature distribution can be resolved and the more accurate the heating can be calculated. However, this also significantly increases the implementation effort and the computing time. A heating calculation with the finite element method (FEM) leads to very good resolutions of the temperature distributions for individual components, if the mesh is appropriately meshed. Thus, the results of a thermal calculation using FEM can be compared with the results of the heat network in order to make a statement as to whether the resolution of the heat network is chosen sufficiently high enough. For this purpose, the same parameters are used for the heat dissipation at the surfaces in both models, so that occurring temperature differences of a static calculation are solely due to heat conduction. The comparison shows a sufficiently high network resolution due to small temperature differences (**Figure 6**).
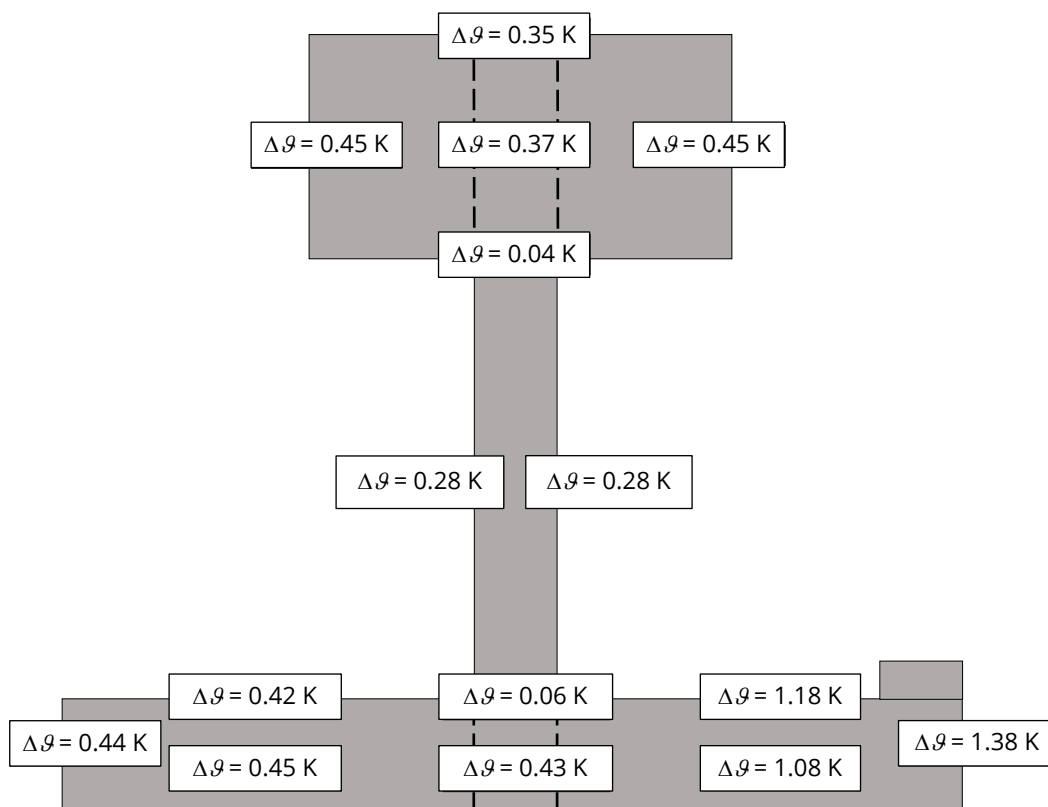

Figure 6: deviation of the calculated steady-state temperature between thermal network model and FEM calculation at selected measuring points

Subsequently, the parameters for heat injection into the rail and heat dissipation via convection and radiation must be determined experimentally. Initial heating experiments show that it is not possible to feed the heating power of the heating rod into the thermal

network using a single power source. On the one hand, radiation and convection on the surface of the heating rod would not be taken into account and on the other hand, the heat input would not take place precisely over the complete contact surface between the foot of the stock rail and the heating rod. Instead, the heating rod is constructed as a separate body. 15 heat power sources generate the heat flow and five thermal nodes realize the contact to the stock rail (**Figure 7**).
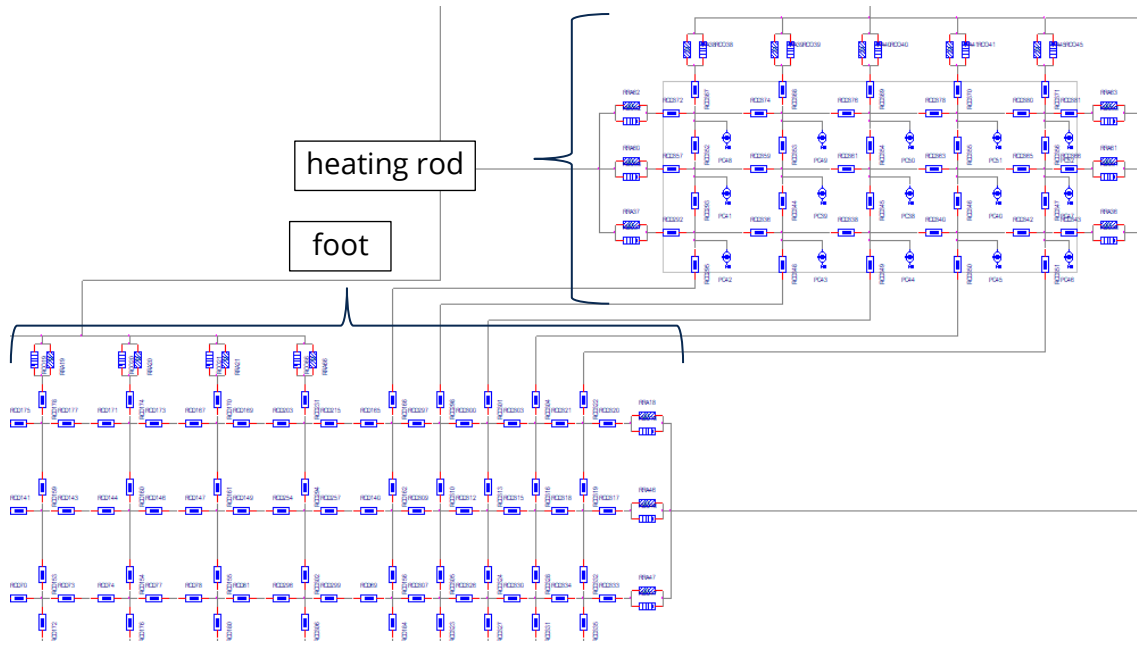

Figure 7: connection between the thermal networks of stock rail foot and heating rod

For the experimental investigation, the heating rod is attached to the stock rail with the existing clamps at first. The heating rod is mounted centrally to the stock rail in the longitudinal direction (l_{rail} = 3.63 m; l_{rod} = 2.90 m). In order to achieve the lowest possible heat transfer from the rail to the floor, the stock rail rests on a 12 cm thick polystyrene layer. The temperatures are measured distributed over the circumference of the rail in three areas (**Figure 8**). One measuring area is located in the longitudinal direction in the middle of the stock rail and the heating rod. The other two measuring areas are arranged at a distance of 0.5 m to the left and right respectively.
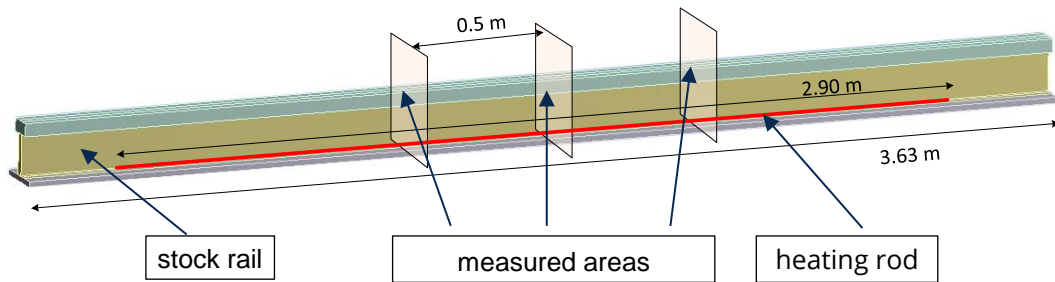
Figure 8: experimental setup of stock rail and heating rod for verification of the thermal model

The three different measuring ranges are intended to average the measured temperatures in order to reduce the effect of measurement errors. The position of the clamps for fixing the heating rod and thus its thermal effect on the heat transfer are clearly visible in the thermographic images of the experiment (**Figure 9**). However, they are not taken into account in the heat network. Instead, the calculation in the heating network calculates an average value of the heat transfer from the positions at a heating rod terminal and the gap.
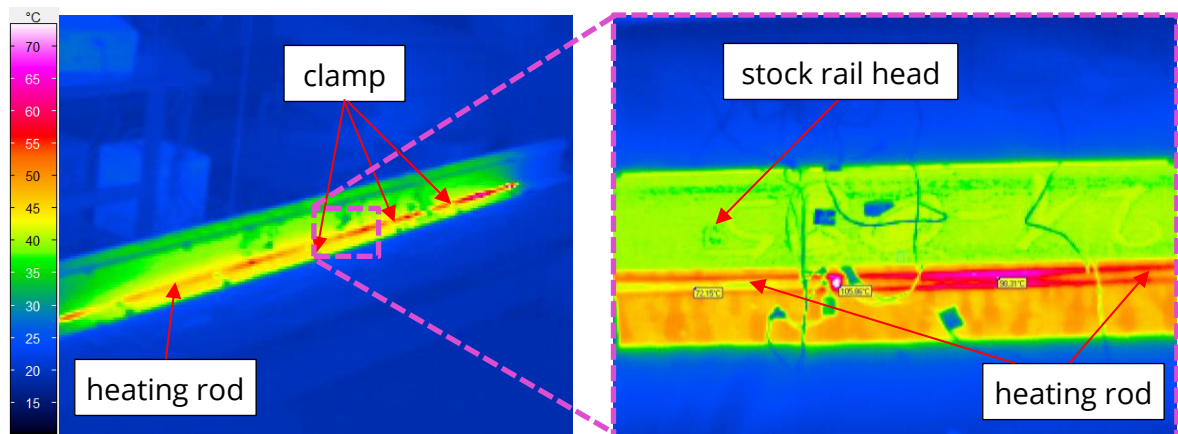

Figure 9: temperature distribution at the heating rod in longitudinal direction measured by a thermal imaging camera

Within one measurement area, thermocouples measure the temperatures at nine positions on the surface of the stock rail and at one position on the heating rod (**Figure 10**). An additional measurement on the surface of the heating rod could not be carried out because the soldered connection on the thermocouple melts due to the high temperatures ($\vartheta > 200$ °C).
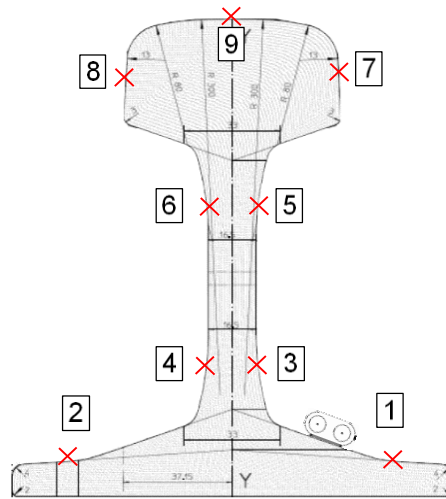
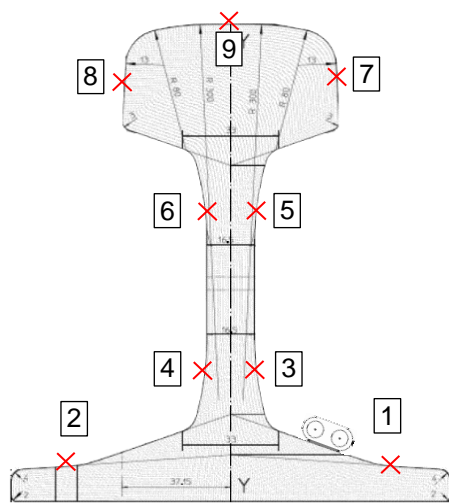Figure 10: numbering of the temperature measurement positions at each area

The temperature measurement positions are distributed over the circumference of the stock rail. A symmetrical arrangement to the vertical axis was chosen to detect a possible temperature difference between the inside and the outside of the stock rail. Thermocouples type K (NiCr-Ni) were used to record the temperatures. They were soldered to copper lamellas (with an area of 1.3 cm²) that we glued to respective positions of the rail (**Figure 11**).

Figure 11: glued copper lamellas with thermocouples on top

Missing thermal parameters like the emissivity for the heat radiation, similarity parameters for the convection and the heat transfer resistance between heating rod and foot of the stock rail can now be determined. To determine the emissivity, the measurement results of a thermal imaging camera are compared with the temperatures measured by the thermocouples. Convection parameters are determined by visualizing the airflow at the rail and the heat transfer resistance between heating rod and rail is determined by a parameter study. A detailed description of this procedure can be found in the 4th interim report **[4]**. In addition, all parameters used for the heating networks of

the stock rail and heating rod are attached to the report (**Attachment 2**). With a heating power P = 900 W and an ambient temperature ϑ_u = 17.1 °C, small differences between measured and calculated temperatures could be determined using the parameters determined (**Figure 12**).

position	Θ_{calc} / °C	Θ_{meas} / °C	$\Delta\Theta$ / K
1	69.8	75.6	5.8
2	63.3	63.5	0.2
3	61.9	58.3	-3.6
4	61.4	58.3	-3.1
5	52.0	50.1	-1.9
6	50.5	50.1	-0.4
7	48.3	45.2	-3.1
8	47.7	45.2	-2.5
9	47.7	45.4	-2.3

Figure 12: measured and calculated temperature rise for an electrical power P = 900 W at an ambient temperature ϑ_a = 17.1 °C

With the complete thermal network of the point, it should also be possible to calculate the heating as a function of time (dynamic). Therefore, thermal capacities have to be implemented in the thermal network. The highest possible accuracy is achieved if each thermal node is connected to a thermal capacity. However, due to the high implementation effort and the relatively high thermal conductivity of the rail material this is not necessary. Special thermal nodes are selected via the cross-section of the stock rail, which represent the heat storage for entire sections. This concerns five nodes in the foot of the stock rail, two in the web and three nodes in the head of the stock rail. The parameters for the density and the specific heat capacity of the rail material are taken from a search for the steel "R350 HT". A dynamic calculation of the heating was carried out exemplarily at the web (**Figure 13**), at the head and at the foot of the stock rail. If one compares the measured and calculated temperatures, only small differences can be seen, so that the number of thermal capacities in the model can be regarded as sufficiently high. The verification of the dynamic heating calculation can be read in more detail in the 5th interim report **[5]**.
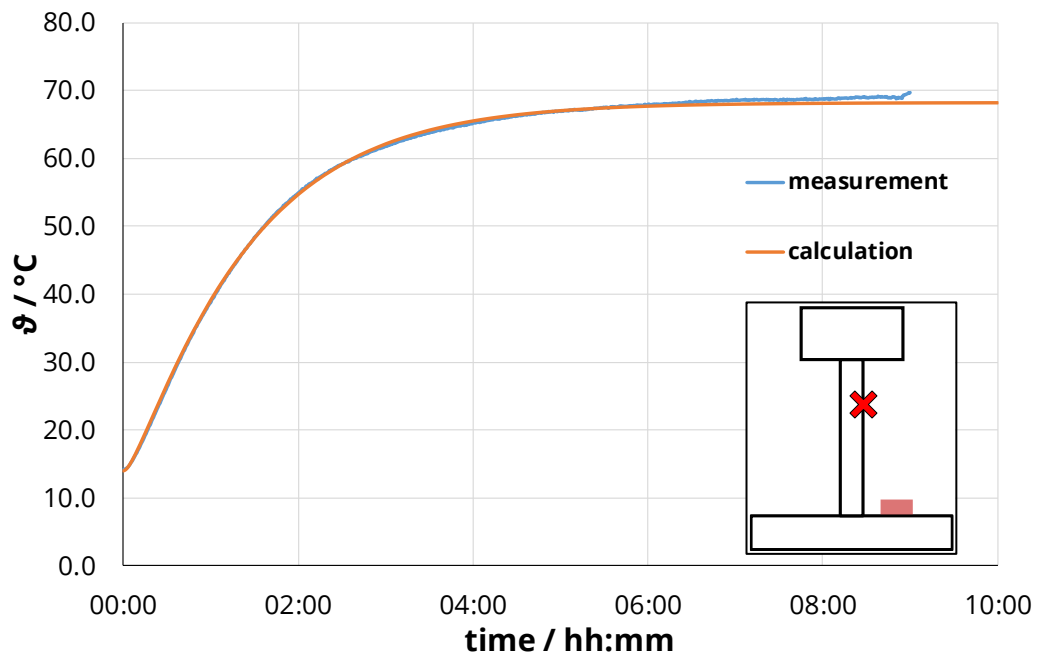
Figure 13: measured and calculated time-depending heating at the web of the stock rail

The heating network of the stock rail is currently able to calculate a two-dimensional heat transport. At a point, however, a three-dimensional heat flow will occur in the stock rail even if the heat is fed homogeneously through a heating rod. This is caused by base plates, which serve as bearing points of the stock rail with a centre distance of 60 cm. The heating network must therefore be extended in the longitudinal direction in order to calculate a longitudinal heat flow. The method with the highest accuracy would also be to use every thermal node from the thermal network of the cross-section for this purpose. Analogous to the implementation of the thermal capacities representative thermal nodes are determined, which realize the connection in longitudinal direction. Thus, the already existing heat network of the stock rail is duplicated several times and the same (representative) nodes are connected by heat conduction resistors (**Figure 14**). Five thermal nodes in the foot, four nodes in the web and two nodes in the head are selected for this purpose.
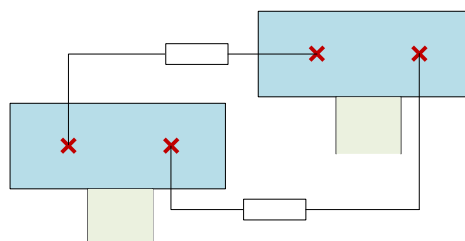

Figure 14: connection of the thermal networks of the stock rail in longitudinal direction (exemplary at the stock rail head)

In the area of the point, the head shape of the stock rail changes to ensure positive contact with the head of the tongue rail. This change in geometry is not taken into account in the thermal model as the effect on heat transfer is considered very small. For the heating calculations, which are finally to be carried out with the thermal model, the area around the point tip is of particular thermal interest. For this reason, a total length of 5.639 m of the point area was thermally mapped for the thermal network. Of these, 1.80 m lie in front of the point tip (i.e. the beginning of the tongue rail) and 3.839 m behind it. It is also important to look at the area in front of the point tip. There the heating will be different from in the area of the point due to the missing tongue rail. The area in front of the point tip therefore clearly influences the heating of the point. In the thermal network model, the first 90 cm are not heated. In the area of the second 90 cm, which borders on the switch point, a heating rod is connected. The area in front of the point tip is called section V. The remaining geometry of the stock rail is defined with the sections A to D (**Figure 15**).
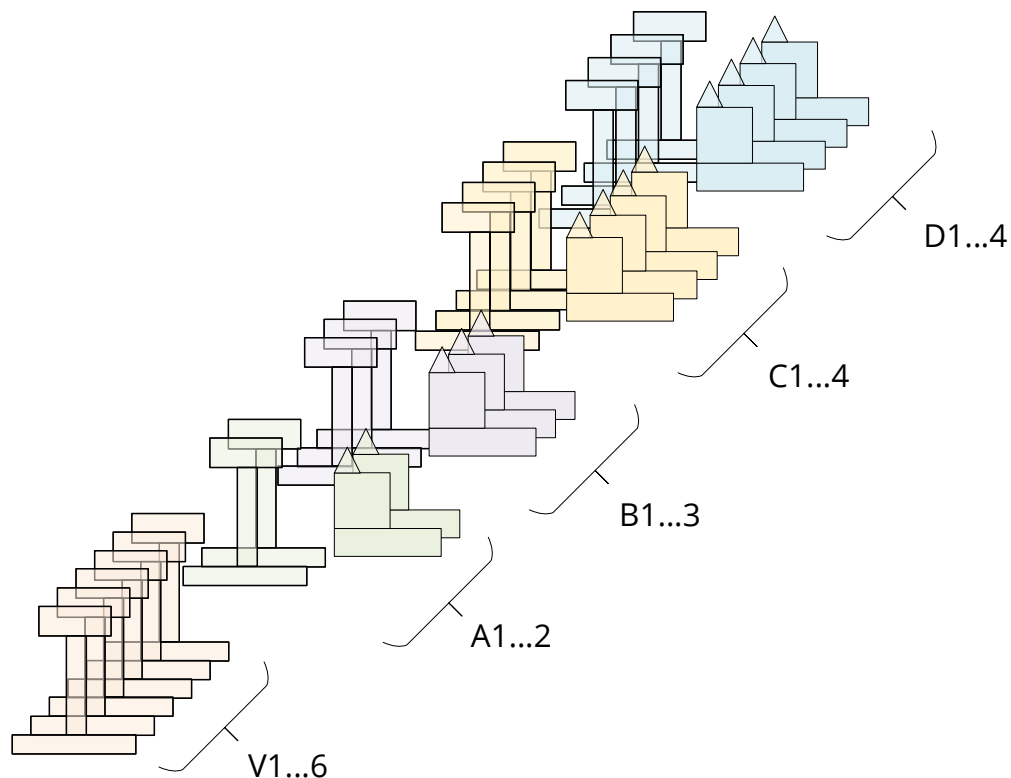

Figure 15: sections and sub-sections of the stock rail

The sections are again divided into sub-sections and marked with a number. Depending on the geometry, the number of sub-sections varies from two to six (**Table 4**). The final designation of a sub-section is made up of the letter of the section and the number. For example, sub-section "B2" describes the middle subsection in section B. The listed length of the sections and sub-sections results from the geometry properties of the tongue rail and applies to a point with a radius R = 500 m (chapter 4.2).

Table 4:   length of sections and subsections of the stock rail

section	length	number of subsections	length of a subsection
V	1800 mm	6	300 mm
A	250 mm	2	125.0 mm
B	880 mm	3	293.3 mm
C	1400 mm	4	350.0 mm
D	1309 mm	4	327.3 mm

4.2   Set up of the thermal network of the tongue rail

The structure of the thermal network of the tongue rail is very similar to that of the stock rail. However, the cross-sectional geometry of the tongue rail in longitudinal direction changes partly quantitatively and qualitatively. The provided technical drawing divides the geometry of a tongue rail for a point radius R = 500 m into sections A to J (**Attachment 3**). As already mentioned for the stock rail, the area around the tip of the point is of primary interest from a thermal point of view. Therefore, only the sections A to D were used in the thermal model (further sections of the tongue rail can be added if necessary). The sections of the tongue rail are divided into sub-sections. The sections, sub-sections, their lengths and positions correspond to those of the stock rail (**Figure 15**, **Table 4**). This means that the sub-sections of the stock rail and tongue rail are based on the technical drawing of the tongue rail. The subdivision into sub-sections was carried out in order to obtain a finer resolution of the thermal network in the longitudinal direction of the rail.

The original geometry of the tongue rail must first be approximated so that it can be implemented in the thermal network. The geometry for the sections A, B and C is similar, so that it can be simplified by a rectangle in the foot and web and a triangle in the head (each related to the cross-section; **Figure 16**). In section D, foot and web are approximated with the same shapes, but the head is approximated by a trapezoid.

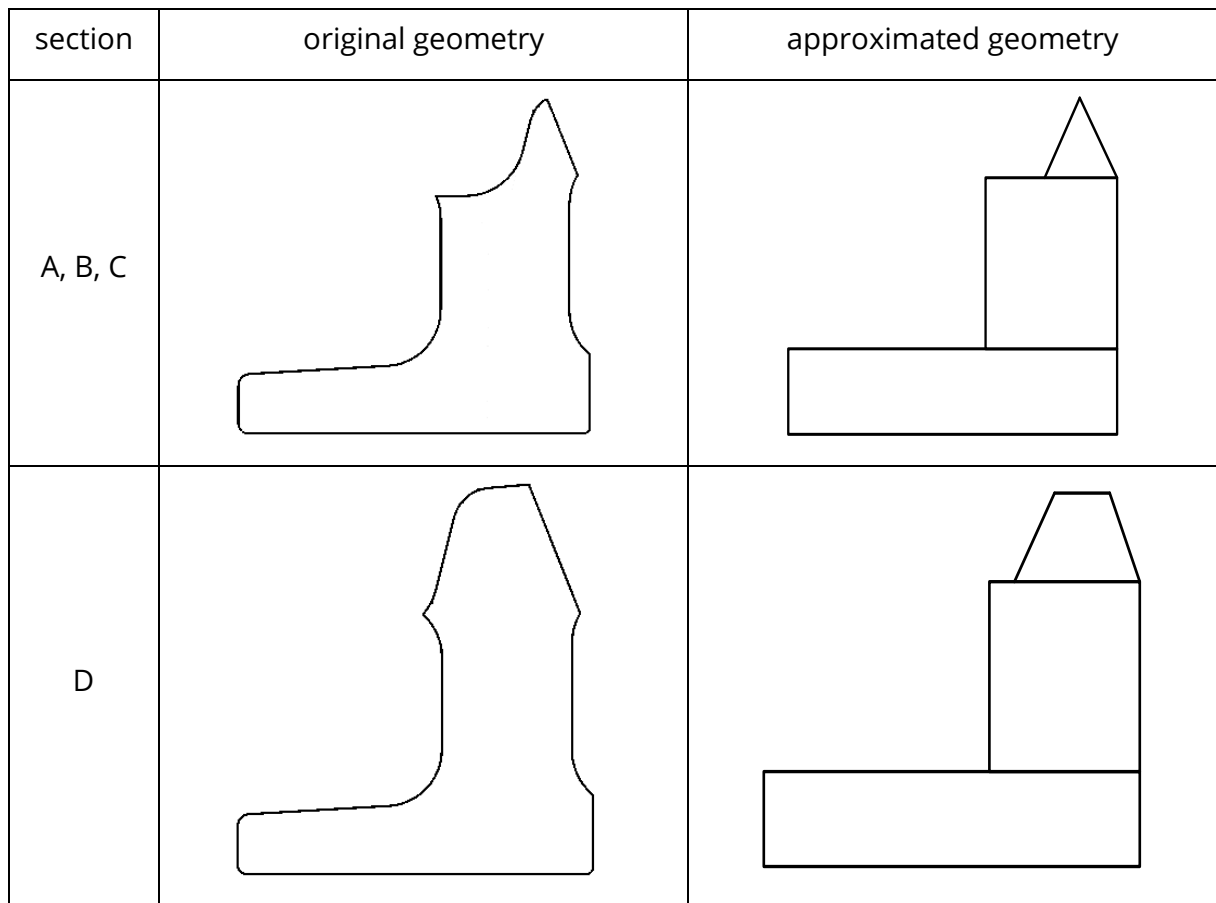| section	original geometry	approximated geometry
A, B, C		
D		

Figure 16: shape of original and approximated geometry for sections A, B, C, D of the tongue rail

A comparison of circumference and area between original and approximated cross-sections shows only minor differences (**Table 5**).

Table 5: comparison between the geometries of original and approximated cross-sections of the tongue rail

cross-section	A_a / A_o	O_a / O_o
A	0.963	1.026
B	0.961	1.026
C	0.958	1.041
D	0.976	1.053

As a result, the difference in volumes and surfaces is also small. The influence of approximation on heat conduction and heat emission is negligible. The approximated geometries are constructed with resistors for heat conduction. At the interface to the environment, resistors for heat radiation and convection are set. A first comparison of a

heating calculation between heat network and FEM showed a maximum temperature difference of 1.6 K with a temperature difference of 100 K between heat input and ambience (see 4th interim report **[4]**). The small temperature difference of both calculation variants confirms a sufficiently high network resolution of the thermal network.

The sub-sections of the tongue rail are linked in longitudinal direction with heat conduction resistors. For this purpose, representative thermal nodes are again determined in the sub-segments. Four nodes in the foot, four nodes in the web and one node in the head are chosen based on the geometric dimensions of the tongue rail (**Figure 17**).
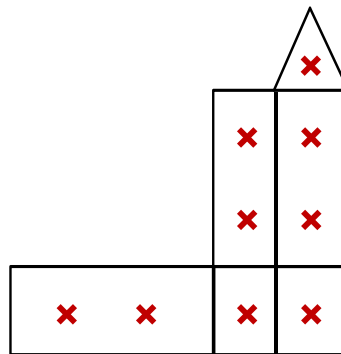

Figure 17: representative thermal nodes for connection of two sub-sections of the tongue rail in longitudinal direction

For the experimental verification of the heat network model of the tongue rail, a rail of the company "Tensol Rail AG" of the type "EW VI-500 TOZ-S -LR" with a length of 3.00 m is available. For this purpose, the existing thermal network of the entire tongue rail must first be reduced to a length of 3 m (measured from the tip). This corresponds to sub-sections A1 to D2. At subsection D2, resistors for convection and radiation are connected to the representative thermal nodes instead of the resistors for heat conduction. Thus, the real conditions of heat emission at the end of the model rail can be simulated.

The heat is fed into the rail by a heating rod with a length of l = 2.90 m and a heating output of P = 900 W at a voltage of U = 230 V. The heat is fed in through a switch heating rod with a length of l = 2.90 m and a heating output of P = 900 W at U = 230 V. The heat transport via the foot to the floor is largely limited by a 12 cm thick polystyrene layer. The temperatures were measured in three areas along the length of the tongue rail. The area in the middle had a distance of 1.50 m to both ends of the tongue rail. The other two measuring ranges were positioned 6 cm in front and 6 cm behind each other (**Figure 18**).
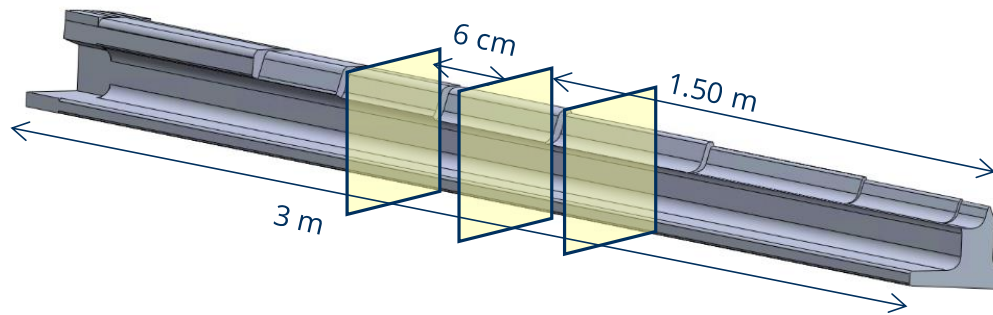
Figure 18: position of the temperature measurement areas at the tongue rail

In order to reduce the influence of random measuring errors, the measured temperatures of the respective measuring points in the different areas should be averaged. For this purpose, the size of the surface used for heat emission should change as little as possible. Therefore, a relatively small distance between the measuring ranges is chosen. The geometry changes only very slightly in this length section and therefore has no influence on the heating. The measuring areas correspond to sub-section C1 in the thermal model.

In each measuring range, seven positions are selected for the temperature measurement (**Figure 19**).
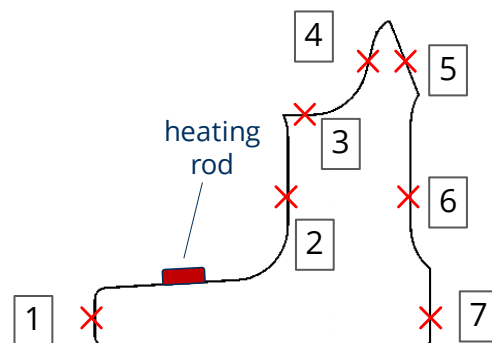

Figure 19: temperature measurement positions within one area of the tongue rail

Temperatures are measured with type K thermocouples. The input power is $P = 400$ W and the temperatures are taken at an ambient temperature of $\vartheta_u = 33.9$ °C ().

Table 6:   comparison of calculated and measured temperatures at the tongue rail

meas. position	ϑ_{TNM} / °C	ϑ_{meas} / °C	$\Delta\vartheta$ / K
1	77.3	75.5	1.8
2	72.9	70.9	2.0
3	72.3	70.5	1.8
4	71.4	69.4	2.0
5	71.4	68.8	1.6
6	72.8	71.1	1.7
7	74.1	71.5	2.6

In the thermally static state, only minor differences between measured and calculated temperatures can be seen on the tongue rail. The parameters for the thermal elements are well chosen. A complete list of the tongue rail parameters can be found in the attachment (**Attachment 4**). The experimental verification can be read in detail in the 5th Interim Report **[5]**.

In order to be able to calculate a time-dependent heating of the tongue rail, thermal capacities are inserted. In each sub-section, there are four capacities in the foot, four capacities in the web and one capacity in the head of the cross-section. The parameters for density and specific heat capacity were set equal to the stock rail.
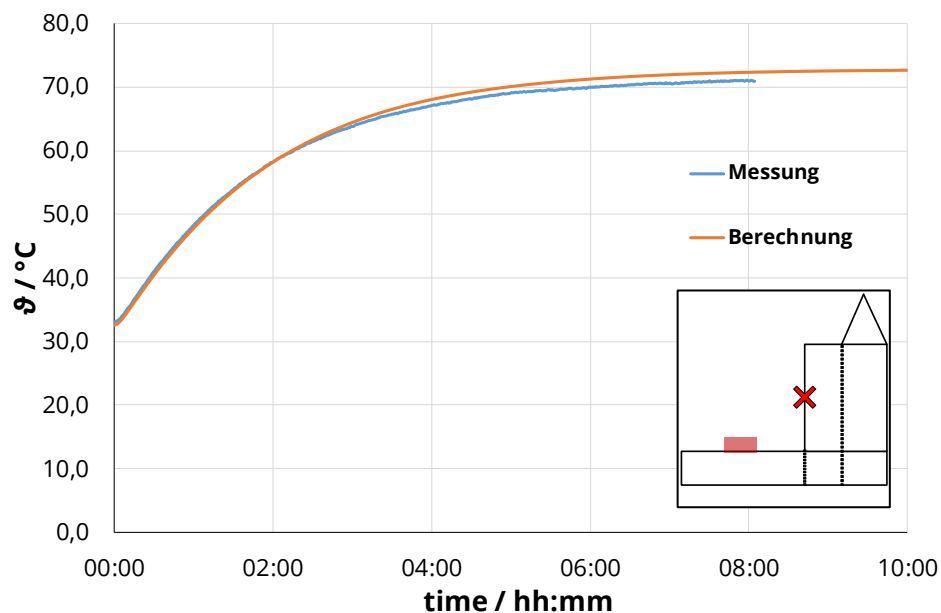

Figure 20: measured and calculated time-depending heating at the web of the tongue rail

The small difference between the calculated and the measured temperatures confirms the accuracy of the installed heating network to calculate a time-dependent heating of the tongue rail (**Figure 20**). Sufficient thermal capacities have been implemented.

4.3   Set up of the thermal network of base plate and slide chair

In principle, the base plate and slide chair can be regarded as one component. The base plate serves to support the stock rail and fasten the rails to the sleeper. The slide chair is the bearing surface of the switch rail, which varies its position depending on the setting of the point (**Figure 21**).

Figure 21: base plate and slide chair mounted on a concrete sleeper

Due to the relatively good thermal conductivity of steel (approx. (15 ... 70) W (m K)$^{-1}$ [1], part of the heat can be conducted from the stock rail to the tongue rail or vice versa via the base plate and slide chair without both components touching directly. It is therefore important for the heating network of the entire point that the base plate and slide chair are also modelled.

The geometry data of the base plate and slide chair were provided by ÖBB based on a technical drawing (**Attachment 5**). The procedure for setting up the heating network is the same as for the stock rail and tongue rail. First, the original geometry of the component is approximated in order to be able to build it up in the thermal network with little effort (**Figure 22**).
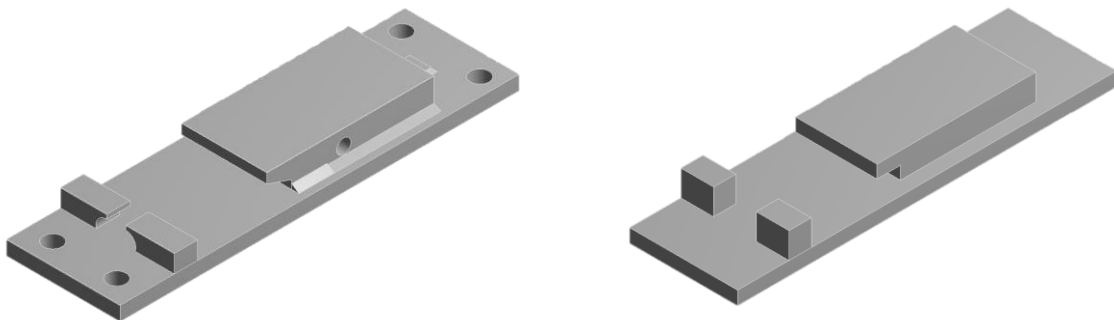

Figure 22: original (left) and approximated geometry (right) of base plate and slide chair

For this purpose, the four screw holes for connection to the sleeper, the recess in the slide chair and the welding seams of the slide chair are removed. The two blocks of the base plate are replaced by simple cuboids and their length and height are adjusted. In order to be able to assess the effect of the approximated geometry on the heating in a first approximation, the size of the surface and the volume of the original and approximated geometry are compared (**Table 7**).

Table 7: comparison of surface and volume between original and approximated geometry of base plate and slide chair

	original geometry	approximated geometry	percentage deviation
surface	0.193 m^2	0.196 m²	1.6 %
volume	2.59 dm³	2.66 dm³	2.7 %

There are only small deviations between the surfaces and the volumes of the original and the approximated geometry. The heat conduction in the component as well as the heat dissipation to the environment is not significantly influenced by the approximation of the geometry.

To confirm this assumption, a FEM calculation is performed. A temperature of ϑ_q = 50 °C on the surface of the sliding chair and an ambient temperature of ϑ_u = 0 °C are defined for this purpose. The calculated temperatures of the FEM model are compared with the calculation results of the heat network (**Figure 23**). The thermal network consists of heat conduction resistors, which simulate the approximated geometry, and resistors for convection and radiation at the interface to the environment. Convection and radiation were implemented identically for both models.
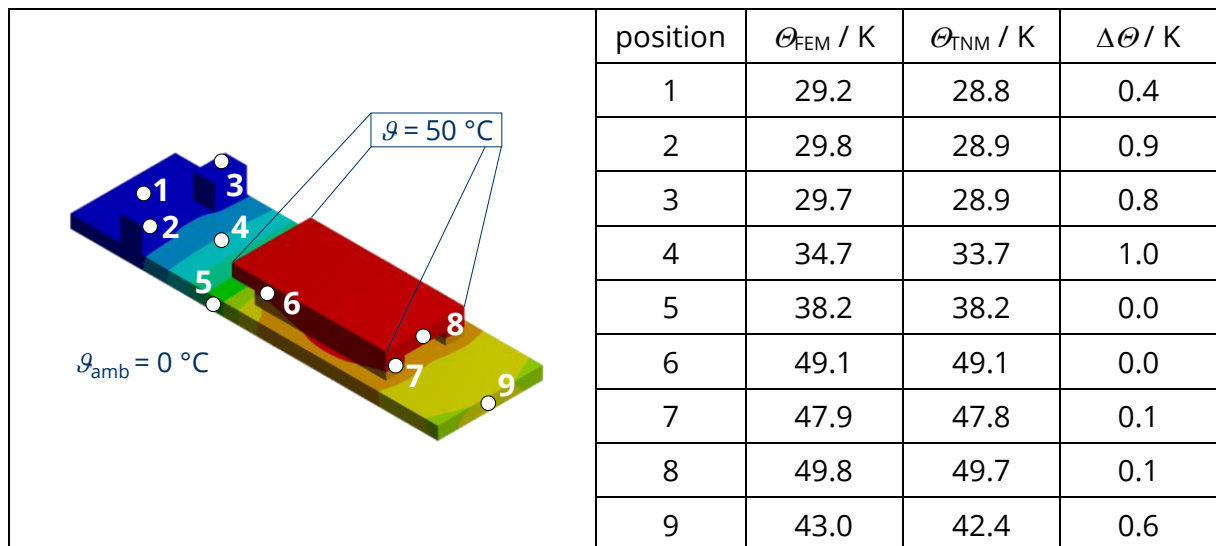

position	Θ_{FEM} / K	Θ_{TNM} / K	$\Delta\Theta$ / K
1	29.2	28.8	0.4
2	29.8	28.9	0.9
3	29.7	28.9	0.8
4	34.7	33.7	1.0
5	38.2	38.2	0.0
6	49.1	49.1	0.0
7	47.9	47.8	0.1
8	49.8	49.7	0.1
9	43.0	42.4	0.6

Figure 23: calculated temperature rise of FEM and TNM model in comparison

The small temperature differences between the heating calculations with the heating network and the FEM model confirm a sufficiently high number of thermal elements in the heating network. In the next step, the selected parameters for heat conduction, convection and heat radiation must be verified experimentally. In order to conduct the thermal energy into the component for the experimental investigation, a heating plate is used. The heating plate is an aluminium cuboid with the dimensions 120 mm x 63 mm x 20 mm. In this cuboid, there are two symmetrical, parallel bores in which heating cartridges are located. The thermal energy is generated in the heating cartridges and distributed evenly along the surface of the heating plate due to the high thermal conductivity of aluminium (approx. 223 W / (m K)$^{-1}$ **[1]**). The heating plate rests on the slide chair or the base plate. An insulation made of rock wool prevents a large heat dissipation from the heating plate to the environment. Two different, separately investigated heat feeds help to determine the necessary network density and make it possible to investigate the heat flow in two different directions. Furthermore, it is also possible to determine the emissivity of the surface covered by the heating plate and insulation (**Figure 24**).
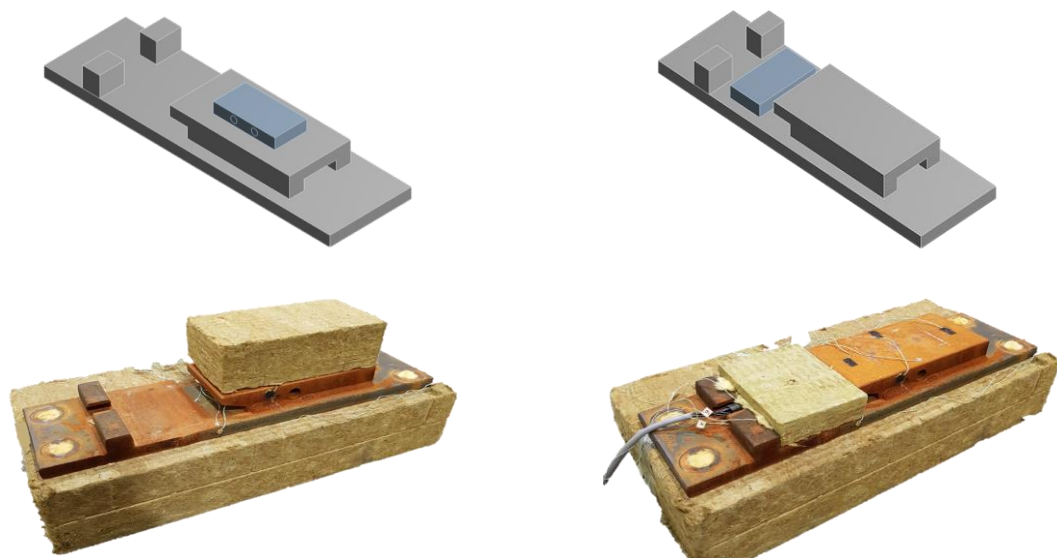

Figure 24: Both positions of heat-input schematic (top) and at experiment (bottom)

In order to achieve the lowest possible heat dissipation to the floor, the base plate is laid on a 12 cm thick layer of rock wool. The parameters for the thermal network for the base plate and slide chair are given in full in the **Attachment 6**. For this parameter selection the largest agreement between calculated and measured temperatures for a static heating could be determined (**Table 8**, **Table 9**).

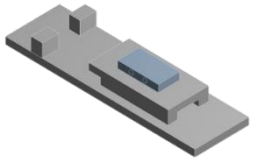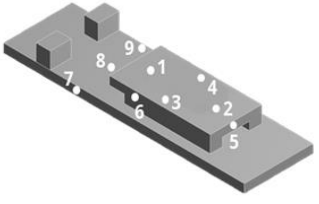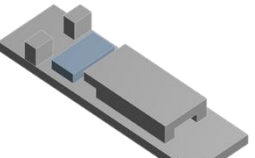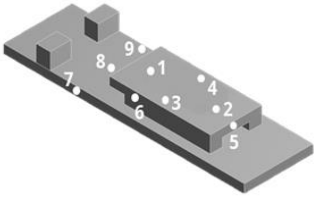Table 8:   measured and calculated temperature rise with heat input at slide chair

	position	Θ_{meas} / K	Θ_{calc} / K	$\Delta\Theta$ / K
	1	62.8	63.4	0.6
	2	62.8	62.8	0.0
	3	63.8	62.3	-1.5
	4	63.1	62.3	-0.8
	5	59.5	61.4	1.9
	6	58.9	60.5	1.6
	7	44.2	45	0.8
	8	45.5	45.2	-0.3
	9	43.7	45	1.3

Table 9:   measured and calculated temperature rise with heat input at base plate

	position	Θ_{meas} / K	Θ_{calc} / K	$\Delta\Theta$ / K
	1	42.2	40.5	-1.7
	2	34.4	35.3	0.9
	3	40	40	0
	4	39.8	39.6	-0.2
	5	34.1	35	0.9
	6	42.7	42.1	-0.6
	7	61.8	63.6	1.8
	8	65.0	65.0	0.0
	9	62.4	63.6	1.2

The differences between the calculated and the measured temperatures in the thermally stationary state are less than 2 K for both positions of the heating element at all measuring positions. The small temperature differences confirm the accuracy of the heating network of the finned plate and slide chair for thermal stationary calculations. The verification can be found in detail in the 5th interim report **[5]**.

For the calculation of time-dependent heating, thermal capacitors are added to the thermal network. Originally, approx. 60 capacitors are implemented for the verification. The temperature and time differences remain small during the comparison. For the final

model, the thermal capacities are reduced to eight capacities in the base plate and four capacities in the slide chair in favour of the computing time. No significant reduction in accuracy can be observed.

4.4   Set up of the thermal network of a sleeper

The sleeper is the link between the heated part of a point and the track bed. In this way, a thermal network of the sleeper provides information on how much heating power is transferred from the rails to the track bed. Due to the almost cuboid shape of the concrete sleeper, only few changes have to be made to the original geometry for the approximation. Only the drill holes for fixing the base plates, the chamfers on the edges and unevenness on the surface are neglected (**Figure 25**). The steel reinforcement is neglected for the construction of the thermal network.
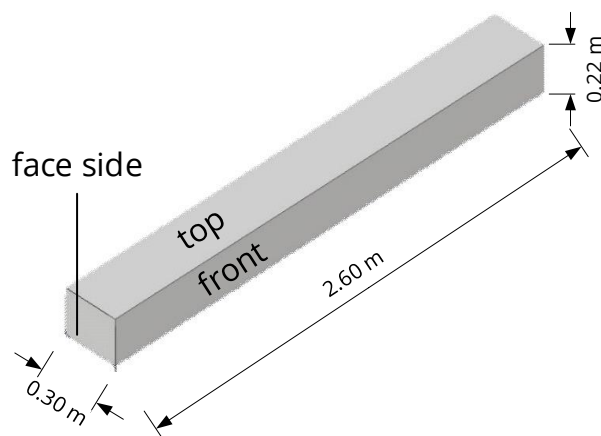

Figure 25: dimensions of the approximated geometry of the concrete sleeper

The homogeneous shape of the geometry allows an uncomplicated construction of the thermal network from resistors for heat conduction, convection and radiation. The thermal parameters for the heat transport processes can be determined with an experimental investigation. The thermal power is fed in via a heating plate measuring 300 mm x 260 mm x 20 mm. The heating plate delivers a maximum power of $P_H = 200$ W. A 12 cm thick rock wool underlay thermally insulates the sleeper against the ground (**Figure 26**).
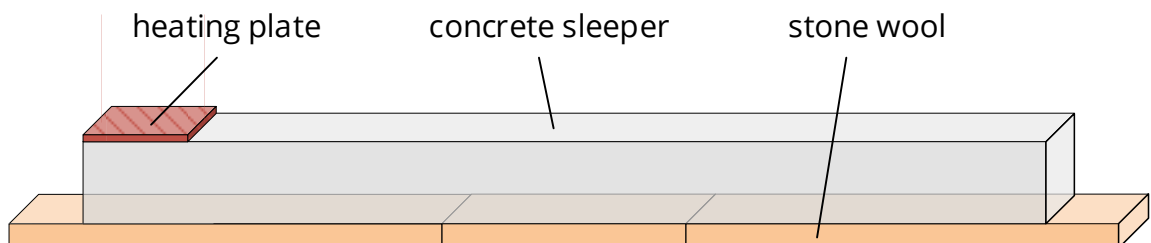

Figure 26: experimental setup for verification of the thermal network of the sleeper

The heating plate is covered on the sides and on the top with a 12 cm thick layer of rock wool in order to guarantee the greatest possible heat input into the sleeper. Type K thermocouples are used to measure the temperature. For the heating test, the heating plate is positioned on the upper side of the sleeper (**Figure 26**). The temperatures are measured at six positions on the top and front sides and at eight positions on the front side of the sleeper (**Figure 27**).
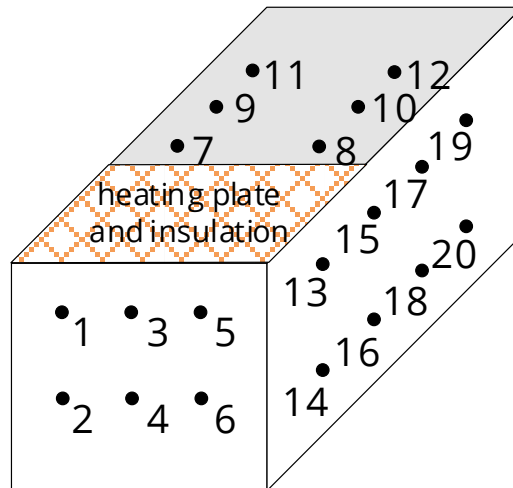

Figure 27: position of the temperature measurement positions at the concrete sleeper

Table 10: comparison of measured and calculated temperatures at the sleeper

pos.	1	2	3	4	5	6	7	8	9	10
ϑ_{exp} / °C	56.1	43.6	64.7	48.5	56.6	44.9	43.2	45.4	31.4	31.5
ϑ_{TNM} / °C	57.0	42.8	60.2	47.5	57.0	42.7	37.0	37.2	28.5	28.6
$\Delta\vartheta$ / K	0.9	-0.8	-4.5	-1.0	0.4	-2.2	-6.2	-8.2	-2.9	-2.9
pos.	11	12	13	14	15	16	17	18	19	20
ϑ_{exp} / °C	26.1	26.5	61.6	47.4	46.5	40.7	31.4	31.3	26.4	26.7
ϑ_{TNM} / °C	25.3	25.3	74.0	51.7	37.1	37.0	28.5	29.4	25.3	25.6
$\Delta\vartheta$ / K	-0.8	-1.2	12.4	4.3	-8.4	-3.7	-2.9	-2.9	-1.1	-1.1

At an input thermal power of P = 100 W and an ambient temperature of ϑ_u = 23.5 °C there are partially clear differences (max. 12 K pos. 13) between the measured and calculated temperatures (**Table 10**).

In addition to deviations in the thermal network model, faulty measurement of the temperature on the thermally low conductive surface of the concrete is also possible. The elaborate optimisation of the thermal network of the sleeper or the temperature measurement at the sleeper is dispensed with, as the accuracy of the thermal network of the sleeper has a lower priority than the thermal networks of the stock rail and tongue rail, as well as the base plate and slide chair. The parameters for the thermal network of the sleeper can be read in the **Attachment 7**.

4.5 Connection of the separate thermal networks to a thermal network of the whole point

A major advantage of the heat network method is the possibility of connecting subnetworks in an uncomplicated way. For this purpose, the thermal nodes of different components are connected to each other via heat conduction or radiation. The transition resistors can be adjusted as required at this point. In comparison, the separate subnetworks have different network resolutions. When connecting the networks, care must be taken to ensure that the network densities in the connection area are adapted to each other. This happens by short-circuiting the thermal nodes of the component with the higher resolution. As an example, this method is shown at the transition from the foot of the stock rail to the base plate (**Figure 28**).
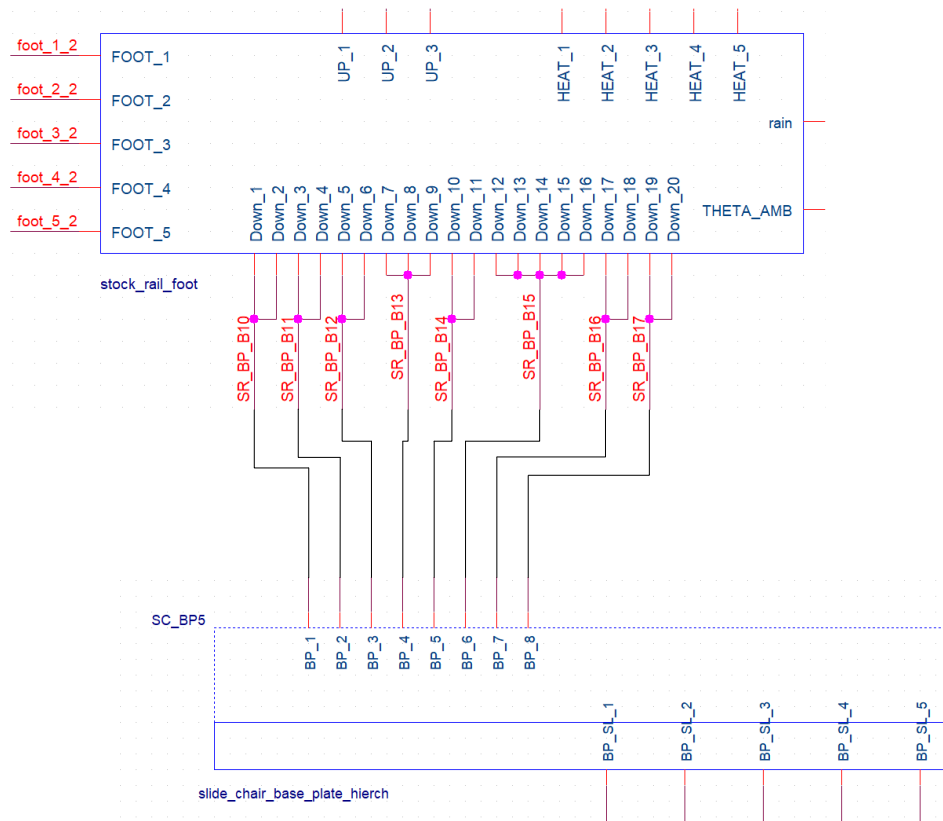

Figure 28: connecting two components of different network resolution by taking the example of stock rail and base plate (displayed simplified)

For the contact surface, 20 thermal nodes are used at the foot of the stock rail and only eight thermal nodes at the base plate. The 20 nodes of the stock rail must therefore be grouped into a total of eight new nodes. However, the spatial spacing of the groups must be taken into account and must correspond to the spacing of the nodes on the base plate. For this reason, either two, three or five thermal nodes were combined to form a group on the stock rail.

In addition to the connection point between the stock rail and the base plate, this method is also used to connect the tongue rail and the slide chair, the base plate and the sleeper as well as the stock rail and the tongue rail (by radiation or radiation and heat conduction; depending on the side of the point).

In addition, thermal resistors are implemented at the transition from stock rail to base plate, from slide chair to tongue rail, from base plate to sleeper and from stock rail to tongue rail. An elastic intermediate plate with a thickness of 4.0 mm is located between the underside of the base plate and the concrete sleeper. For the specific thermal conductivity, an average value for elastomers was chosen and λ = 0.2 W m^{-1} K^{-1} **[2]**. Due to the low conductivity of the concrete of the sleepers, it is not necessary to thermally model the complete sleeper, but only the area in which heat conduction still takes place. Therefore, only one-half of the sleeper is considered at the respective position in the thermal network. For heating under laboratory conditions, resistors for convection and radiation are connected to the thermal nodes on the complete surface of the concrete sleeper, which is not covered by the base plate. For the heating calculation of the real point, it was assumed that the sleepers would be laid up to half the height in the track bed. The upper half of the sleeper is connected to thermal resistors for convection and radiation and the thermal nodes of the lower half are connected to temperature sources at ambient temperature potential.

Another important consideration is the arrangement of the components in the longitudinal direction of the point. As already shown in **Figure 15**, the stock and tongue rails are divided into sub-sections in the longitudinal direction. The sleepers and also the base plates and slide chairs each have a centre-to-centre distance of 60 cm. This means that not every subsection can be linked with the base plate, slide chair and sleeper. These components must therefore be assigned to the sub-sections that are in the correct position (**Attachment 8**). It was determined that sub-section A1 is at the height of a sleeper.

The number of modelled components in the thermal network and the respective network resolution reduce the clarity of the point model. A variant to eliminate this circumstance is a hierarchical structure of the thermal network. The thermal network of the point is structured in three hierarchical levels (**Table 11**).

Table 11: assignment of the hierarchical setup of the thermal model of the point

layer 1	- overview of all components - implementation of global parameters that can be adjusted depending on the ambience factors - sections of the rails are displayed
layer 2	- overview of the separate sub-sections of the rails - overview of base plate and slide chair - implementation of local parameters of single components or sections and global parameters that do not have to be adjusted - fine resolution of the sleeper
layer 3	- fine resolution of foot, web, and head of stock rail or tongue rail - fine resolution of base plate or slide chair

To enable a hierarchical structure, a part file had to be created for each component from the respective thermal network. These components are stored in various libraries (**Attachment 9**).

For the heating calculation of the X-side of the point, there is a heat exchange via radiation between the stock rail and the tongue rail. However, since one surface does not completely envelop the other, not the complete part of the emitted radiation reaches the other component. In order to calculate the actual heat radiation involved in the heat exchange between stock rail and switch rail, a shape factor must be determined. The shape factor indicates the proportion of the exchanged thermal radiation to the entire radiated heat (**eq. (14)**, **[6]**).

For simplification, the inner web and the inner side of the head of the stock rail, as well as the head, web and foot of the tongue rail on the inner side are determined for the mutual radiation exchange. Furthermore, it is assumed that the radiating surfaces are parallel and infinitely long. Under these conditions, the shape factor can be calculated in a simplified way (eq. (16)).

$$F_{12} = \frac{1}{2x}\left[\sqrt{(x+y)^2+4} - \sqrt{(y-x)^2+4} \right] \tag{16}$$

with $x = \dfrac{h_{SR}}{s}$ and $y = \dfrac{h_{TR}}{s}$; where h_{SR} or h_{TR} is the height of the radiation surface of stock rail or tongue rail and s is the distance between both surfaces. The calculation of the shape factor between stock rail and tongue rail was carried out separately for each section due

to the geometrical changes of the tongue rail (**Table 12**). The distance between both surfaces is s = 180.5 mm.

Table 12: shape factors for the X-side at rail distance of s = 180.5 mm

section	h_{SR}	h_{TR}	F_{12}
A	155 mm	108 mm	0.266
B	155 mm	111 mm	0.273
C	155 mm	118 mm	0.290
D	155 mm	125.5 mm	0.306

In the heating calculation of the Y-side of the point, it is assumed that the head of stock rail and tongue rail are in direct contact with each other in sub-sections A1, A2, B1 and B2. From sub-section B3 onwards, there is a narrow gap between the respective head of the two components. For the subsections A1, …, B2 heat conduction takes place via the head and heat radiation via the web of stock rail and tongue rail. Here the shape factors are assumed to be simplified with F_{12} = 1. For the sub-sections B3 … D4, the gap between the head of stock rail and tongue rail is very small. The heat radiation transferred from one component to the other is divided between the link web-web and head-head. The shape factor between the webs is again simplified with F12 = 1. The view factors for the head-head connection were calculated depending on the respective geometry of the subsection and the gap width (**Table 13**). The values for the gap width are taken from measurements at the model point under outdoor conditions in Chelles.

Table 13: shape factors for the head of stock and tongue rail at the Y-side

section	s	$h_{h, SR}$	$h_{h, TR}$	F_{12}
A	0.00 mm	heat conduction		
B1; B2	0.00 mm	heat conduction		
B3	0.05 mm	31.95 mm	31.95 mm	0.998
C	0.50 mm	38.75 mm	38.75 mm	0.987
D	1.00 mm	44.26 mm	44.26 mm	0.978

For the radiation exchange between two components, a simple radiation resistor is used in the thermal model. The radiation resistor is parameterised with the emissivities of both surfaces and the product of the involved surface with the corresponding shape factor.

5 Verification of the thermal network by means of a model point

The experimental investigation at a model point in the laboratory offers the opportunity to verify the composite heat network without the influence of different environmental conditions (changing ambient temperature, solar radiation, wind, precipitation). For this

purpose, a model point from a supplier of Infrabel with a length of 1.86 m is available (**Table 14**). The model point differs in some points from the definition of the EuroPoint. A major difference is the presence of a hollow sleeper with the lock of the point. The hollow sleeper is made of metal. Experimental investigations must show whether the hollow sleeper causes a different heat transport between both sides of the point or to the ground.

Table 14: list of the components of the model point for the heating under laboratory conditions

component	type	amount	length / mm
stock rail	UIC 60	2	1860
tongue rail	UIC 60 flexible switch shaped part on the top	2	1550
point lock	CDP clamp lock WKV 50-2 Bharat Forge CDP GmbH without motor drive	1	
hollow sleeper	hollow sleeper for WKV 50-2 lock (e.g. VS-BF)	1	
sleepers	concrete (centre to centre ca. 600 mm) in accordance with ÖBB	2	
slide chair and slide plate	Schwihag BGL 606 with IBAV and insulated bolts	4	
base plate	base plate with insulated bolts (in accordance with Infrabel)	2	
roll system	Schwihag/CDP	4	

The heating power is brought into the point by means of electrical point heating rods from Türk Hillinger with a related power of 300 W/m. Thereby both sides of the point (X-side and Y-side, see **Figure 2**) are heated separately and together. Thermocouples of type T measure the temperatures. The temperature measurement at selected points shows that no significant heat transport from one side of the point to the other occurs (**Table 15**, **Table 16**).

Table 15: measured temperatures at Infrabel point with heated X-side at thermally static state (ϑ_{amb} = 24.0 °C)

	measurement position	temperature	temp. rise
X-side	stock rail head top	54.5 °C	30.5 K
	stock rail foot inside	70.5 °C	56.5 K
	tongue rail web (facing stock rail)	30.5 °C	6.5 K
	hollow sleeper (middle)	23.3 °C	-0.7 K
Y-side	stock rail head top	23.1 °C	-0.9 K
	tongue rail web (facing stock rail)	23.2 °C	-0.8 K

Table 16: measured temperatures at Infrabel point with heated Y-side at thermally static state (ϑ_{amb} = 22.3 °C)

	measurement position	temperature	temp. rise
Y-side	stock rail head top	57.1 °C	34.8 K
	stock rail foot inside	42.4 °C	20.1 K
	tongue rail web (facing stock rail)	45.5 °C	23.2 K
	hollow sleeper (middle)	23.5 °C	1.2 K
X-side	stock rail head top	22.9 °C	0.6 K
	tongue rail web (facing stock rail)	23.3 °C	1.0 K

It can be seen that even in the middle of the sleeper no significant temperature rise occurs. Furthermore, the components on the non-heated side of the point reach ambient temperature. When using a concrete sleeper instead of a hollow sleeper made of metal, there is a larger cross-sectional area but a significantly lower thermal conductivity, so that a similar result would be expected. Both sides of the point are to be regarded as thermally decoupled. Thus, the thermal model can be divided into two different models, one for each side of the point. The result is two models with higher clarity and less computing time.

Furthermore, it is noticeable that the heat transfer from stock rail to tongue rail is much higher at the Y-side of the point than at the X-side. At the Y-side, the heat transport is favoured by heat conduction and larger visibility factors of the heat radiation. Further findings can be read in detail in the 5th interim report **[5]**.

The temperature measurements can then be compared with the calculations of the thermal network. The measurement with heated X-side is used to compare the temperatures on the X-side and analogously the measurement with heated Y-side for the comparison with the Y-side. For the X-side, eight positions are available for comparison (**Figure 29**).
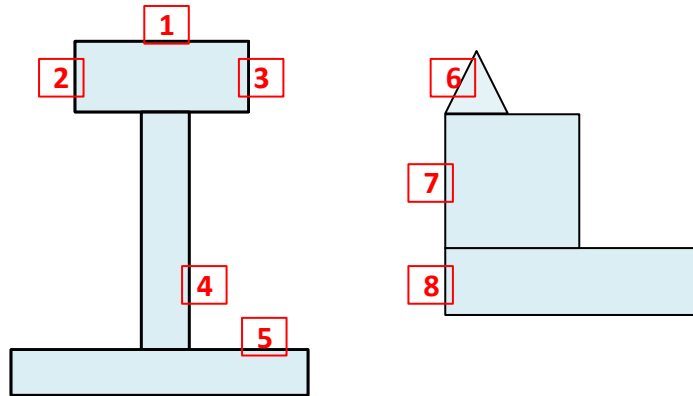

Figure 29: positions for the comparison of measured and calculated temperatures at the X-side of the Infrabel point

With the measured ambient temperature ϑ_{amb} = 24 °C the thermal calculation is also carried out. The thermal resistance between the foot of the stock rail and the base plate or between the foot of the tongue rail and the slide chair is determined experimentally to $R_{th, SB}$ = 0.375 K/W or $R_{th, TS}$ = 0.833 K/W. As an approximation, the resistors with these values are parameterized uniformly for all subsections involved. The comparison shows a relatively good agreement between calculated and measured temperatures (**Table 17**).

Table 17: comparison between calculated and measured temperatures at the X-side of the Infrabel point

pos.	1	2	3	4	5	6	7	8
ϑ_{meas} in °C	54.5	54.2	54.9	62.8	70.5	30.5	30.5	30.3
ϑ_{calc} in °C	56.4	56.3	56.4	61.4	69.0	32.4	32.2	32.7
$\Delta\vartheta$ in K	1.9	2.1	1.5	- 1.4	- 1.5	1.9	1.7	2.4

For the Y-side of the point, other comparison positions on the rails are selected (**Figure 30**).
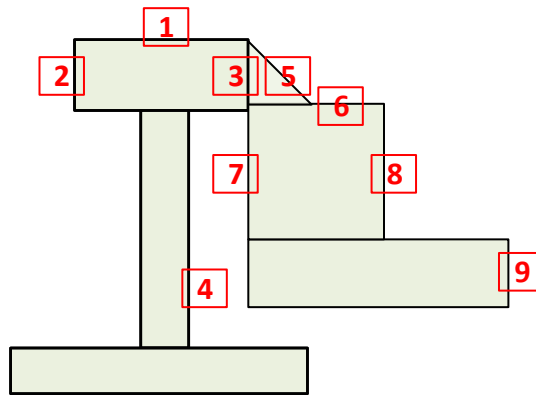
Figure 30: positions for the comparison of measured and calculated temperatures at the Y-side of the Infrabel point

The measurement of the temperatures and the calculation are performed at an ambient temperature of ϑ_{amb} = 23.1 °C (**Table 18**).

Table 18: comparison between calculated and measured temperatures at the Y-side of the Infrabel point

pos.	1	2	3	4	5	6	7	8	9
ϑ_{meas} in °C	57.1	56.3	53.1	68.0	44.6	43.8	45.5	43.8	42.4
ϑ_{calc} in °C	58.6	58.4	58.6	64.8	44.2	44.1	44.4	44.1	43.0
$\Delta\vartheta$ in K	- 1.5	- 2.1	- 5.5	3.2	0.4	- 0.3	1.1	- 0.3	- 0.6

The relatively large temperature difference at the point of contact between the head of the stock rail and the head of the tongue rail is striking. These deviations may have been caused by both the measurement and the calculation. Due to unevenness of the surfaces, the heads of stock rail and tongue rail do not touch each other ideally. In addition, due to its geometric dimensions, the mounted thermocouple changes the gap width and thus also the heat transfer between the two components of the point. The temperatures measured at this point in the test are significantly influenced by these two factors and can therefore differ significantly from the calculated temperatures.

The thermal network model is also highly accurate for time-dependent heating calculations (see the 5th interim report **[5]**). Environmental parameters can now be implemented in the thermal network to be able to calculate heating processes under outdoor conditions.

6 Implementation of the ambient factors into the thermal network

To calculate the heating under outdoor conditions, the influence of the environmental parameters air temperature, wind direction, wind speed, global radiation, precipitation in the form of rain or snow must be taken into account. With the complete TNM model of the point, it makes sense to assume more critical conditions for the calculation. Thus, a certain reserve for implementation errors can be maintained when estimating the effectiveness of the heating system. The parameter global radiation can theoretically increase the temperatures at the point. However, it is important to estimate its influence in advance to increase the accuracy of the verification of the heating network under outdoor conditions.

The ambient temperature is already implemented in all elements in the thermal network model and can be adjusted as required using a global parameter "theta_amb". For wind speed, a field in the parameterisation of the resistors for convection is already provided. However, the parameters c_2 and n_2 have to be determined first (**eq. (8)**). The components are assigned similarity parameters of adequate arrangements from literature.

6.1   Wind speed and direction of wind

The air moves more slowly at lower altitudes than at higher altitudes due to friction with the ground. The wind speed v_2 can be calculated dependent on height if a measured value with the corresponding measuring height h_1 is known (**eq. (17)**) **[7]**.

$$v_2 = v_1 \left(\frac{h_2}{h_1} \right)^g \tag{17}$$

The size of the exponent g depends on the surrounding terrain **[8]**. In the heating experiment under outdoor conditions (see next chapter) the wind speed was measured at a height of $h_1 = 1.60$ m. The thermal nodes of the point components jaws, tongue rail, base plate and slide chair are located on average at a height of $h_2 = 0.15$ m. With a terrain exponent $g = 0.28$ for a terrain with smaller obstacles, the following results are obtained

$$v_2 \approx 0.5 \, v_1 \tag{18}$$

Furthermore, the convective effect of the wind depends on the angle of the airflow. If an axis with an angle of 0 ° is placed along the track, the greatest convective effect occurs at an angle of attack of $\phi = 90$ ° or $\phi = 270$ °. Depending on the respective flow angle, the size of the Nusselt number is reduced (**eq. (19)**) **[9]**. The reduction factor k is added to the heat network as global parameter "angle_corr".

$$Nu_\phi = Nu \cdot k = Nu \cdot \left[0.75 + 0.25 \cos(2\phi + 180) + 0.06 \left| \sin(2\phi) \right| \right] \tag{19}$$

The wind speed in the space between stock rail and tongue rail at the Y-side of the point is assumed to be 5 % of the actual wind speed. The parameter "wind_inside" is used for this. For the remaining convection resistors wind is described with the parameter "wind_speed".

6.2 Global radiation

Under cloudy skies, it can be simply assumed that the temperature for the radiation exchange between component and environment is equal to the temperature of the surrounding air. In cloudless skies, however, these temperatures differ. The radiation exchange takes place between the point components and the higher atmospheric layers. The temperature of the higher layers can be calculated from the ambient temperature ϑ_{amb} (**eq. (20)**) **[10]**.

$$\vartheta_{atmos} = 0.0561 (K)^{-1} \left(\vartheta_{amb} + 273.15\,K \right)^{1.5} - 273.15\,K \tag{20}$$

Thus, it is possible that an unheated rail at night with a cloudless sky can assume a lower temperature than the ambient temperature. If this scenario shall be calculated, the parameter "theta_atmos" must be used.

During the day, thermal power is brought into the switch by radiation from the sun. The amount of the introduced power depends, among other things, on the cloudiness, the elevation of the sun, the azimuth related to the components of the point and the degree of absorption of the components. The global radiation measured in the field test had to be multiplied by a factor of 0.15 in order to parameterize the heat input correctly. This can be read in more detail in the 6th interim report **[11]**. The measured global radiation is described in the heat network model with the parameter "global rad".

6.3 Rain

Precipitation in the form of rain can cool the components of a point directly through heat conduction processes. On the other hand, the point components can also release thermal energy through the evaporation of the water. In case of snowfall, additional thermal energy is required for heating and melting the snow. It cannot be determined by what temperature the water on the rail is heated before it evaporates or runs off the rail. Furthermore, the relationship between water running off and evaporating is also unknown. The thermal energy required for the evaporation process can come from the point or the ambient air. Here, too, it is not known in what ratio the two source media are in relation to each other. Due to these considerations and the superposition of the different processes, the implementation into the thermal network is extremely complicated. The aim is to find an approximation with which rain as well as snowfall can be considered in the thermal network.

Therefore, a rain test under laboratory conditions is carried out first. For the time being, the point heats up to the static final temperature. Then both sides of the point, each individually in separate tests, are sprinkled with a system and the temperatures are evaluated. Only a precipitation quantity of approx. $5\,l\,(m^2 h)^{-1}$ is considered, which corresponds to heavy rain. The water temperature corresponds to 20.5 °C in both partial tests.

Table 19: temperature reduction while sprinkling the X-side of the point

		stock rail			tongue rail		
	ϑ_{amb} / °C	head	web bottom	foot	head	web	foot
ϑ_{dry} / °C	28.2	57.2	65.4	73.1	34.9	35.1	33.7
ϑ_{wet} / °C	27.8	27.6	36.4	42.4	21.9	22.5	21.7

Table 20: temperature reduction while sprinkling the Y-side of the point

		stock rail		tongue rail		
	ϑ_{amb} / °C	head	web bottom	web top	web inside	foot
ϑ_{dry} / °C	28.2	59.5	69.9	33.3	47.6	45.1
ϑ_{wet} / °C	28.4	27.6	36.9	22.3	26.7	24.8

The temperature of the wet point is measured after about five hours of sprinkling. It can be seen that the temperature at the head of the stock rail is reduced to approximately ambient temperature by the sprinkling. Even lower temperatures occur at the tongue rail because the water temperature is also about 8 K below the air temperature. Up to now, there are no thermal elements for calculating the cooling by precipitation or evaporation. However, the process is reminiscent of an open cooling circuit as a technical implementation. This is implemented by means of a master and a slave resistor in the Orcad Capture. In the master resistor, the cross-sectional area of the cooling medium, the flow rate and the temperature of the cooling medium are parameterised. In the slave resistor, the associated master resistor is generally defined. The parameters cross-sectional area and flow rate are not known for the application of a sprinkled point and must be determined in parameter studies (**Table 21**). The parameters for the sprinkling of the X-side of the point are determined and adopted for the Y-side.

Table 21: comparison of calculated and measured temperatures at the X-side while sprinkling the point

		stock rail			tongue rail		
		head	web	foot	head	web	foot
dry	ϑ_{meas} / °C	57.2	65.4	73.1	34.9	35.1	33.7
	ϑ_{calc} / °C	58.5	61.3	65.1	35.1	35.2	35.6
wet	ϑ_{meas} / °C	27.6	36.4	42.4	21.9	22.5	21.7
	ϑ_{calc} / °C	27.6	36.9	43.4	21.3	21.2	21.9

The differences between calculated and measured temperatures are relatively small. Therefore, the choice of parameters is suitable to approximate the thermal effect of rain on the switch. Rain can be switched on (= 1) or off (= 0) as global parameter "rain" in the thermal network on the overview layer.

6.4 Snowfall

For an effective operation of a point heater, temperatures higher than 0 °C must be present at stock rail, tongue rail and slide chair. Fallen snow on these components must be melted. This process can be divided into three sub-processes:

1. Heating up the snow to melting point

2. Melting process

3. Cooling by the water on the rail

It is assumed that the snow initially has ambient temperature. This means that a temperature of $\vartheta_u < 0$ °C energy must be used to heat a mass of snow to 0 °C. The energy requirement is calculated using the specific thermal capacity c of ice (**eq. (21)**).

$$E_{heat} = c \cdot m \cdot \Delta \vartheta \qquad (21)$$

For the melting process itself, the energy requirement is calculated using the melting enthalpy H (**eq. (22)**).

$$E_{melt} = m \cdot \Delta H \qquad (22)$$

The amount of snowfall is generally indicated in the unit height per time (cm / h). Based on the time specification, the respective energy requirement can be converted into a power requirement. The mass of snow is determined from the volume and density of the

snow. An average value is chosen as density. The volume is calculated from the height and the surface of the rails or the slide chair where it is assumed that snow will accumulate.

In the thermal network, the heating and melting process of snow is represented by heat power sources, which carry heat out of the point system. The parameterisation is done on the top layer as a global parameter ("melting_power_stock", "melting_power_tongue", "melting_power_slide"). The parameters can be determined for stock rail, tongue rail and slide chair with the help of the corresponding Excel document.

The third sub-process of snow on the point is the cooling effect of the water after the melting process. This is considered similar to the thermal effect of rain. However, the amount of snow still has to be put in relation to the amount of rain investigated. This is realized in each case via the mass of water. The cooling circuit was verified in chapter 6.3 with a rainfall quantity of about $5\,\mathrm{l\,(m^2h)^{-1}}$. Due to the difference in density, this corresponds to a snow quantity of $50\,\mathrm{l\,(m^2h)^{-1}}$ and thus a snowfall of $5\,\mathrm{cm\,(h)^{-1}}$. Depending on the actual snowfall quantity, parameter "rain" is scaled in the thermal network. The Excel table also calculates the corresponding value. The cooling water temperature is parameterised with 0 °C.

Under certain environmental parameters, problems can occur with this method. If the temperature at the rails or slide chair is lower than 0 °C, the components are heated by the cooling water circuit instead of cooled, as the cooling water has a higher temperature. Therefore, for each calculation scenario one variant with activated and one with deactivated cooling water circuit must be calculated, whereby the lower temperature at the respective point is considered correct.

7 Verification of the thermal network with a point under outdoor conditions

A SNCF point at the Chelles test site in the Paris metropolitan area is available for experimental studies under outdoor conditions. The design of the point is strongly oriented to the definition of the EuroPoint [**3**]. Türk Hillinger heating elements with a power of $P' = 300\,\mathrm{W\,m^{-1}}$ and a length of $l = 3.00$ m are installed at the foot of the stock rails. Three heating elements are placed flush with each other. Thus, the rail is heated as far as possible evenly in the measuring range as well as in the adjacent areas. The temperatures are measured in the area of the sleeper and the slide chair at a distance of 0.85 m from the tip of the point. The supply voltage is lower than 230 V and thus a power of 900 W per heating rod cannot be achieved.

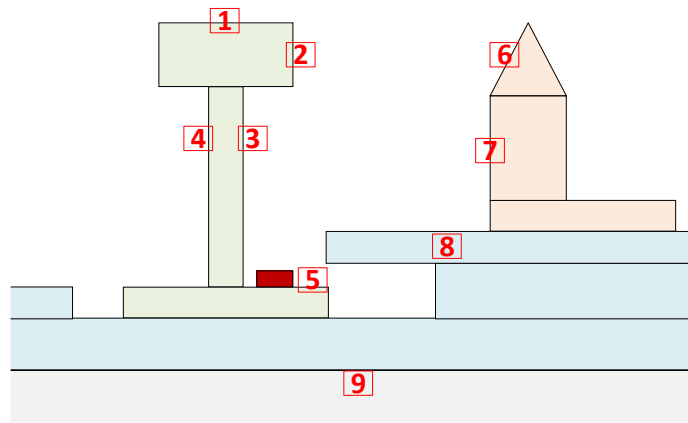Type T thermocouples record the temperatures at nine different positions (**Figure 31**).

Figure 31:temperature measurement positions at the point under outdoor conditions

The environmental parameters are recorded with a weather measuring station. The weather station detects the ambient temperature, wind speed and direction, precipitation and global radiation.

A total of four heating tests are carried out, two on the X-side and two on the Y-side of the point (measurement 1, measurement 2; each). This provides the possibility to investigate the heating for different environmental conditions and thus improve the accuracy of the thermal model. Since the environmental conditions are constantly changing, it is extremely difficult to investigate the dynamic heating behaviour. It is much easier and more accurate to find a time range with environmental parameters as constant as possible in the recorded measurement interval, in which the temperatures can be considered approximately static. Furthermore, the mean values of the variables over two hours before the actual measuring point are used as ambient parameters in the thermal network (**Table 22**). In this way, minor changes in the ambient conditions can be compensated. For all measurements for the static verification no precipitation occurs.

7.1 Comparison at the X-side of the point

Table 22: comparison between measured and calculated temperatures at the X-side under outdoor conditions, measurement 1

model input		results			
parameter	value	position	ϑ_{meas} / °C	ϑ_{calc} / °C	$\Delta\vartheta$ / K
ϑ_{amb}	12.8 °C	1	33.4	35.4	-2.0
P_{electr}	278 W/m	2	32.4	35.4	-3.0
global radiation	250 W/m²	3	34.4	37.0	-2.6
wind	1.2 m/s	4	38.8	36.9	1.4
k-factor	0.93	5	42.1	46.7	-4.6
$R_{th,SB}$	0.375 K/W	6	21.4	18.8	2.6
$R_{th,TS}$	0.833 K/W	7	21.0	18.8	2.2
		8	23.3	25.6	-2.3
		9	13.9	14.5	-0.6

The differences between calculated and measured temperatures are small. The greatest deviation is at the foot of the stock rail (position 5). The thermocouple could only be mounted there offset in the longitudinal direction due to the narrow gap between stock rail and slide chair. The heating element is attached to the foot of the stock rail with a clamp every 30 cm. In the areas of these clamps, the contact pressure of the heating rod is greater and there is a better heat transfer into the stock rail. An inhomogeneous temperature distribution along the surface of the base of the stock rail in the longitudinal direction occurs. Measuring point 5 is closer to a clamp. This would explain the relatively high temperature deviation at this position.

Measurement 2 is performed overnight. This explains the very small amount of global radiation (**Table 23**).

Table 23: comparison between measured and calculated temperatures at the X-side under outdoor conditions, measurement 2

model input		results			
parameter	value	position	ϑ_{meas} / °C	ϑ_{calc} / °C	$\Delta\vartheta$ / K
ϑ_{amb}	9.2 °C	1	27.1	25.5	1.6
P_{electr}	278 W/m	2	26.3	25.5	0.8
global radiation	2.3 W/m²	3	28.3	27.1	1.2
wind	1.7 m/s	4	31.1	27.1	4.0
k-factor	0.85	5	36.5	37.4	-0.9
$R_{th,SB}$	0.375 K/W	6	13.0	11.2	1.8
$R_{th,TS}$	0.833 K/W	7	13.0	11.2	1.8
		8	21.1	18.9	2.2
		9	9.5	10.3	-0.8

The differences between calculated and measured temperatures are relatively small. The largest temperature difference occurs on the outside of the web of the stock rail (measuring point 4). The measured temperature there is also approx. 3 K higher than on the inside of the web (measuring point 3). For design reasons, measuring point 4 is shifted a few centimetres in the longitudinal direction relative to measuring point 3. The measurement shows that this difference in length is thermally significantly noticeable. In contrast, the temperatures calculated with the thermal network show almost no differences between the inside and outside in the upper area of the web of the stock rail.

7.2 Comparison at the Y-side of the point

For the investigation of the Y-side, the point is switched, so that no additional thermocouples have to be attached. Measurement 1 again shows the greatest deviation between measured and calculated temperatures on the outside of the web of the stock rail (measuring point 4, **Table 24**).

Table 24: comparison between measured and calculated temperatures at the Y-side under outdoor conditions, measurement 1

model input		results			
parameter	value	position	ϑ_{meas} / °C	ϑ_{calc} / °C	$\Delta\vartheta$ / K
ϑ_{amb}	11.6 °C	1	33.4	30.5	2.9
P_{electr}	270 W/m	2	28.2	29.6	-1.4
global radiation	70.5 W/m²	3	36.0	34.1	1.9
wind	1.3 m/s	4	39.1	34.0	5.1
k-factor	1.00	5	46.2	46.6	-0.4
$R_{th,SB}$	0.313 K/W	6	31.1	29.6	1.5
$R_{th,TS}$	0.417 K/W	7	26.2	27.9	-1.7
		8	25.1	27.1	-2.0
		9	12.1	13.6	-1.5

At the remaining temperature measuring points the difference is small $\Delta\vartheta$ < 2.9 K. The thermal transfer resistors from the stock rail to the base plate $R_{th,SB}$ and from the slide chair to the tongue rail $R_{th,TS}$ differ slightly from thermal transfer resistor values of the thermal network model for the X-side of the point. The reason for that is that the movement of the tongue rail changes its bearing surface. At the same time, it is possible that the pressure of the tongue rail against the stock rail may slightly change the inclination of the base of the stock rail and thus influence the heat transfer.

The second measurement also shows only slight differences between measured and calculated temperatures ($\Delta\vartheta$ < 2.3 K; **Table 25**).

Table 25: comparison between measured and calculated temperatures at the Y-side under outdoor conditions, measurement 2

model input		results			
parameter	value	position	ϑ_{meas} / °C	ϑ_{calc} / °C	$\Delta\vartheta$ / K
ϑ_{amb}	10.7 °C	1	26.8	26.1	0.7
P_{electr}	273 W/m	2	25.9	25.3	0.6
global radiation	355 W/m²	3	28.5	29.7	-1.2
wind	4.4 m/s	4	31.5	29.7	1.8
k-factor	0.80	5	40.3	42.5	-2.2
$R_{th,SB}$	0.313 K/W	6	27.4	25.3	2.1
$R_{th,TS}$	0.417 K/W	7	26.1	23.8	2.3
		8	22.6	23.5	-0.9
		9	14.2	11.9	2.3

It is noticeable that the temperature at the connection of both rails is lower at the head of the stock rail (measuring point 2) than at the head of the tongue rail (position 6). The heat transport from the heating rod to measuring point 2 is only via heat conduction within a component. There is also heat transfer to measuring point 6. Therefore, it would be expected that the temperature at the head of the tongue rail is lower than at the head of the stock rail. It can be assumed that the measurement of one or both temperatures is faulty. Due to the mounting technique of the thermocouples, e.g. at measuring point 2, the actual thermocouple is closer to the reed rail and only the copper flake is close to the stock rail. Thus, the temperature of the reed rail could dominate the measurement signal.

8 Calculation scenarios of the railway companies

Part of the EuroPoint project was the calculation of different scenarios of environmental conditions based on the interests of the participating railway companies. In mutual consultation, calculation scenarios of ÖBB, SBB and ProRail were examined (**Table 26**). The temperatures in the rails are determined in each case in subsection B2. For each scenario, the temperature distribution on the X-side and the Y-side of the point was calculated.

Table 26: calculated heating scenarios of the railway companies (scenarios with stock rail web insulation in bold)

	scenario no.	ambient temperature	wind speed.	snowfall
ÖBB; 330 W m⁻¹	1	0 °C	24 km h⁻¹	30 cm in 12 h
	2	0 °C	30 km h⁻¹	40 cm in 12 h
	3	0 °C	30 km h⁻¹	30 cm in 12 h
	4	0 °C	30 km h⁻¹	50 cm in 12 h
	5	-5 °C	50 km h⁻¹	10 cm in 12 h
	6	-5 °C	10 km h⁻¹	50 cm in 12 h
	7	**-5 °C**	**10 km h⁻¹**	**50 cm in 12 h**
	8	-5 °C	24 km h⁻¹	10 cm in 12 h
	9	**-5 °C**	**24 km h⁻¹**	**10 cm in 12 h**
	10	-10 °C	24 km h⁻¹	-
	11	**-10 °C**	**24 km h⁻¹**	**-**
SBB; 300 w m⁻¹	1	0 °C	-	-
	2	0 °C	-	heavy rain
	3	0 °C	-	30 cm in 12 h
	4	0 °C	15 km / h	30 cm in 12 h
	5	0 °C	30 km / h	30 cm in 12 h
	6	-5 °C	-	-
	7	-5 °C	-	30 cm in 12 h
	8	-5 °C	15 km / h	30 cm in 12 h
	9	-5 °C	30 km / h	30 cm in 12 h
	10	-10 °C	-	-
	11	-10 °C	-	30 cm in 12 h
	12	-10 °C	15 km / h	30 cm in 12 h
	13	-10 °C	30 km / h	30 cm in 12 h
ProRail; 500 W m⁻¹	1	0 °C	19.4 km / h	10 cm in 10 h
	2	-5 °C	28.4 km / h	-
	3	-10 °C	38.5 km / h	-
	4	-10 °C	38.5 km / h	10 cm in 10 h

8.1   Calculation of the ÖBB scenarios

Heating calculations are performed for a heating power of 330 W/m. Three of the different eleven calculations are carried out with consideration of a stock rail insulation. This insulation covers parts of the foot and web on the outer side of the stock rail. The insulation must be constructed as a separate component to be able to map two-dimensional heat flows within the insulation. A connection in the longitudinal direction is not necessary, since the heat flows in the longitudinal direction are considered negligible due to the low thermal conductivity. The dimensions of the insulation are available as a technical drawing. First the geometry of the insulation must be approximated (**Figure 32**).
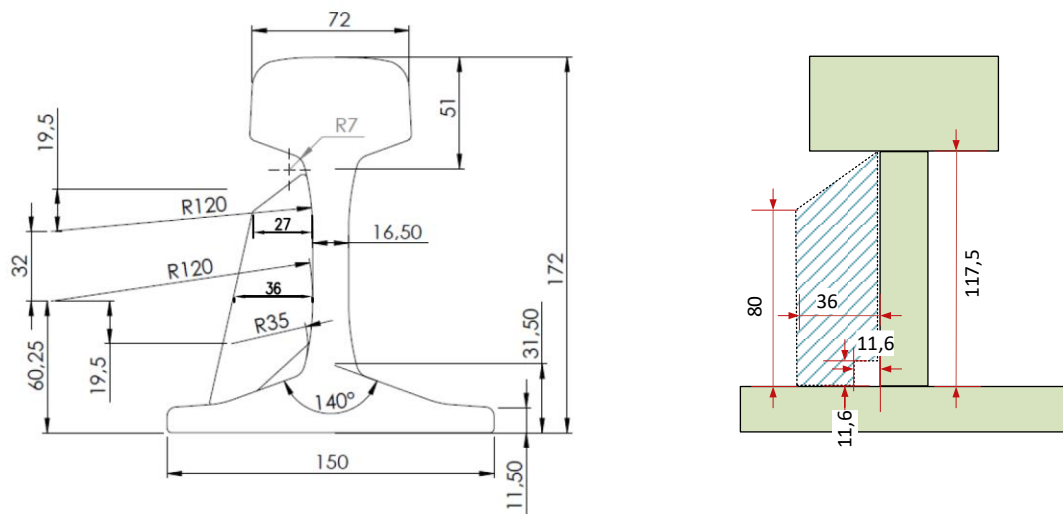
Figure 32: original (left) and approximated (right) geometry of the stock rail insulation

When comparing both sides of the point, lower temperatures can generally be found on the X-side (**Attachment 10**, **Attachment 11**). On the X-side, almost no temperature rise can be detected on the tongue rail in all scenarios. In general, wind and snowfall significantly reduce the temperatures at the point. For each calculation scenario, the temperatures at the tongue rail and at the slide chair are less than 1 °C. Therefore, for the X-side, no further error-free setting of the point can be guaranteed under any of the scenarios examined. The insulation of the stock rail provides for slightly higher temperatures. However, the temperature rise does not increase by more than approx. 30 %. The influence of the insulation can be seen more clearly near the web of the stock rail than at positions further away. The further away the measuring position is from the stock rail insulation, the smaller is the influence on the temperature increase.

On the Y-side, the temperature at the tongue rail is on average approx. 0 °C for all calculated scenarios and is thus significantly higher than on the X-side. Nevertheless, only in scenario 9 a minimum temperature of 1 °C is reached at all measuring positions. Only in this case, it can be assumed that setting the point is possible without restrictions. Here, too, the use of a stock rail insulation causes only a slight increase in temperature.

8.2 Calculations of the SBB scenarios

Compared to the previous scenarios, heating elements with an output of 300 W/m are used here. At an ambient temperature of 0 °C, precipitation is in principle possible in the form of snow or rain. The effects on the warming of both variants (heavy rain and snowfall) were compared (**Attachment 12**, **Attachment 13**). On the X-side, the temperatures at the stock rail are about 1 K lower for rain than for snowfall. On the tongue rail, there is no significant difference in the resulting temperatures. The amount of water in heavy rain is significantly larger than in the examined amount of snow (30 cm in 12 h) and thus the amount of water dominates the melting enthalpy with respect to the thermal influence. On the Y-side, a similar behaviour is shown. Here, the difference at the stock rail is 0.5 K and thus smaller, because when the stock rail and tongue rail are in contact with each other, only a smaller part of the rail surface can be influenced by the precipitation than on the X-axis.

On the X-axis, no significant temperature rise on the tongue rail is observed during snowfall even without the additional influence of wind. At the stock rail, the temperature rise is reduced by about half if the wind speed increases by 15 km/h in addition to snowfall. Only in scenario 1 can a further faultless setting of the point be guaranteed with certainty.

On the Y-side, even at 0 °C ambient temperature and snowfall, a temperature above 1 °C can be reached at all considered positions. Even with an ambient temperature of – 5 °C and snowfall, the temperatures at the point are not significantly lower. A wind speed of 30 km/h causes only extremely low temperature rises at the tongue rail.

8.3 Calculation of the ProRail scenarios

Here, a significantly higher heating power than previously used (500 W/m) is considered. On the X-side, the temperatures at the tongue rail under the influence of 1 cm snowfall per hour and wind at 19.4 km/h are approx. 0 °C (**Attachment 14**). In calculation scenarios 2 and 3 only wind but no snowfall is considered. Nevertheless, no significant temperature rise is noticeable on the tongue rail. Comparing scenario 3 with scenario 4 it becomes clear that with the same wind and ambient temperature, additional snowfall does not cause a significant reduction in temperatures at the point. On the X-side, no scenario can guarantee that the point will continue to be set correctly.

The situation is different on the Y-side. In scenarios 1 and 2, temperatures significantly higher than 0 °C occur at all considered positions (**Attachment 15**). Only for the scenarios with an ambient temperature of – 10 °C an error-free operation of the point cannot be guaranteed.

9 Analysis of the heat flows

An analysis of the heat flows offers the possibility to evaluate heat conduction within the components and the heat emission to the environment. In the previous chapter, it was shown that especially the temperatures at the tongue rail and on the slide chair were low and therefore snow and ice can accumulate at these places first. The aim of the investigation of the heat flows is to find the reasons for the low temperatures in these areas and to identify optimisation potentials. For this purpose, the heat flows that occur between components or sub-components are initially determined on both sides of the point. Environmental conditions and the stock rail insulation already mentioned in the previous chapter are taken into account (Table 27).

Table 27: boundary conditions for the analysis of heat flows

ambient temp..	wind	precipitation	insulation
-10 °C	-	-	-
-10 -°C	15 km/h	-	-
-10 °C	-	-	yes
-10 -°C	15 km/h	-	yes

The heat flows are determined in subsection B2. The subsection has a length of 29.3 cm and is connected to a base plate, slide chair and sleeper. On the Y-side, the tongue rail and stock rail are in direct contact. In the following explanations, differences in the thermal power conducted in and out are caused by longitudinal heat conduction in stock rail and tongue rail. These are neglected in the following because of the clarity and the low relevance.

9.1 Heat flows at the X-side

In windless conditions, a high proportion of thermal power (approx. 89 %) is transported by the heating element into the stock rail (**Figure 33**). Most of the power is transferred from the foot of the stock rail into the base plate. About half of the heat that is transported into the base plate is transferred to the sleeper and is thus no longer available for heating the other point components. The radiation exchange between stock rail and tongue rail is very low at about 1.5 %. So, only approx. 9 % of the total heat reaches the tongue rail.
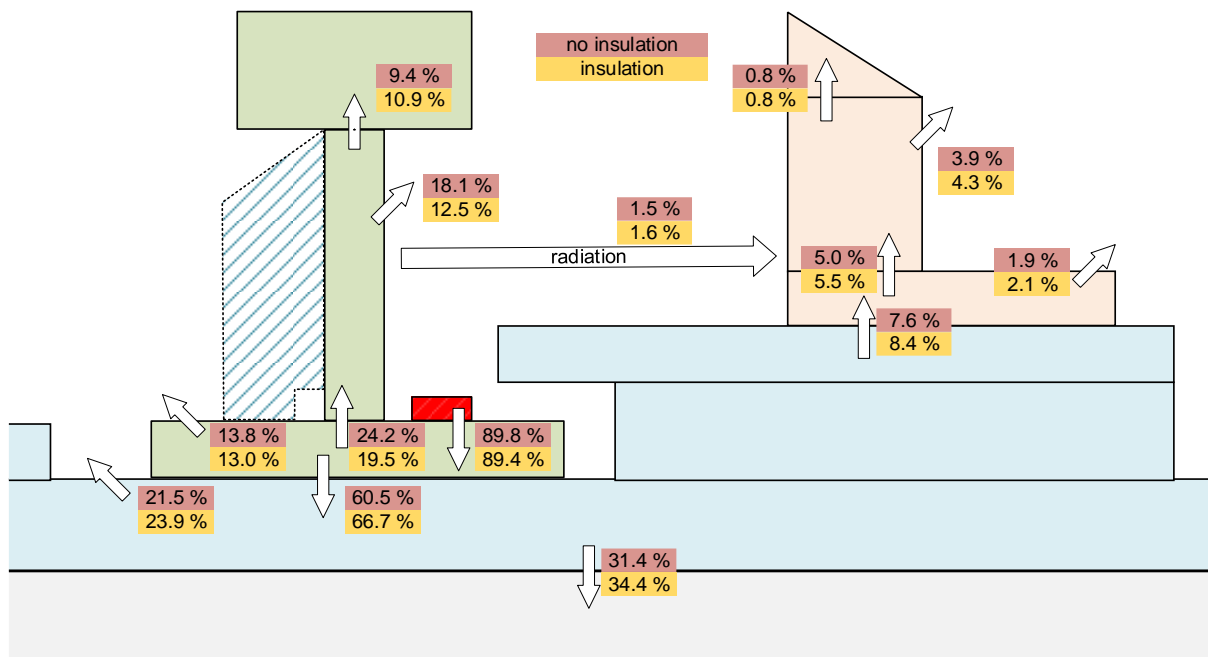
Figure 33: percentage of heat flows to total thermal power at ϑ_u = -10 °C; P = 300 W/m; no wind; no precipitation; on X-side with and without stock rail insulation (straight arrows indicate heat transfer between components; diagonal arrows indicate heat dissipation)

If a stock rail insulation is additionally attached to the outside of the web, the heat flows change quantitatively, but not qualitatively. Due to the lower heat dissipation from the web of the stock rail, less heat is conducted into the web and instead into the base plate. Only a very small portion of this additional heat reaches the foot of the tongue rail. The majority is either dissipated by the base plate and slide chair to the surroundings or conducted into the sleeper. This explains why an additional insulation at the web of the stock rail hardly influences the temperatures.

For wind with a speed of 15 km/h the heat flows change significantly (**Figure 34**). Less than approx. 70 % of the generated heat is transported from the heating rod into the foot of the stock rail. Compared to windless conditions, less than half of the heat is transferred from the foot of the stock rail to the base plate. The heat transfer from the base plate to the sleeper is also significantly lower. Only 4 %... 5% of the heat output provided by the heating rod reaches the tongue rail.
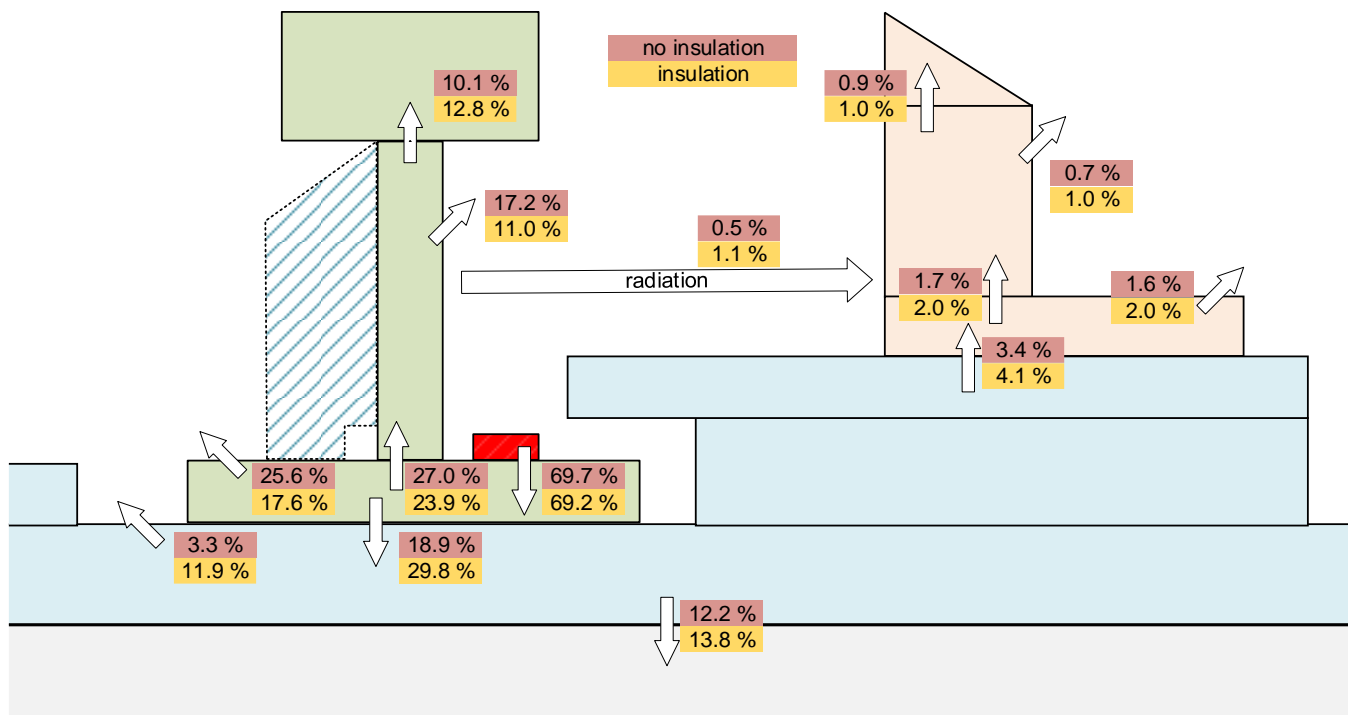
Figure 34: percentage of heat flows to total thermal power at ϑ_u = -10 °C; P = 300 W/m; 15 km / h wind; no precipitation; on X-side with and without stock rail insulation (straight arrows indicate heat transfer between components; diagonal arrows indicate heat dissipation)

Here the stock rail insulation has a similar effect as in the investigation without wind influence. A slightly lower proportion of the heat is conducted into the web of the stock rail. On the other hand, the percentage of heat that is transported from the foot of the stock rail to the base plate is greater. Due to the heat dissipation to the environment and to the sleeper, the amount of heat that reaches the tongue rail differs only imperceptibly from the arrangement without stock rail insulation.

9.2   Heat flows at the Y-side

On the Y-side of the point, the heat flows differ significantly from those on the X-side. In windless conditions, however, a similarly high proportion of heat (approx. 90 %) is initially conducted from the heating element into the foot of the stock rail (Fig. 35). In the variant without insulation, more heat is conducted into the web of the stock rail than on the X-side. At the head of the stock rail, heat is conducted to the head of the tongue rail. Approx. 22 % of the generated power is transferred in this way. The heat transfer from the base plate to the sleeper is similar to that on the X-side with approx. 35 %. On the X-side, the head of the tongue rail was the heat sink of the essential components of the point. In this scenario, it is the base plate with slide chair. This means that the lowest temperatures occur there at the point (apart from the sleeper) and the heat flows are directed there.

The share of radiation in the heat exchange between stock rail and tongue rail is again about 1%, so in this case it is almost negligible compared to heat conduction.
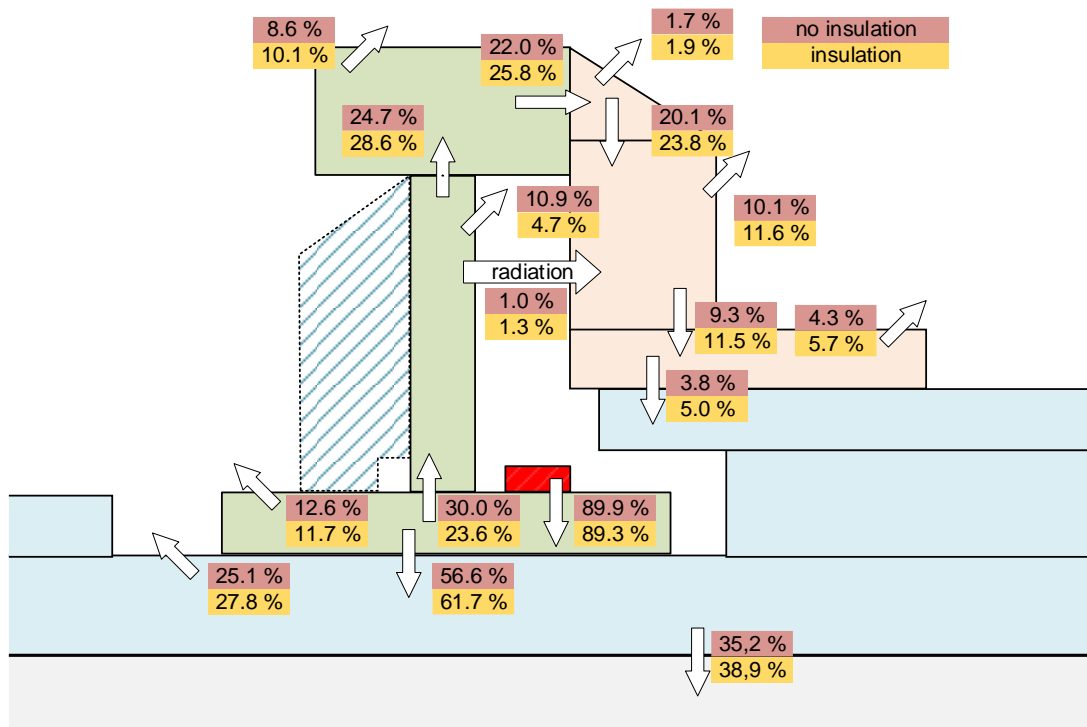
Figure 35: percentage of heat flows to total thermal power at ϑ_u = -10 °C; P = 300 W/m; no wind; no precipitation; on Y-side with and without stock rail insulation (straight arrows indicate heat transfer between components; diagonal arrows indicate heat dissipation)

The stock rail insulation reduces the heat emission from the foot and web of the stock rail. The additional heat is transferred to the other components. In the tongue rail, however, the heat flows differ only slightly.
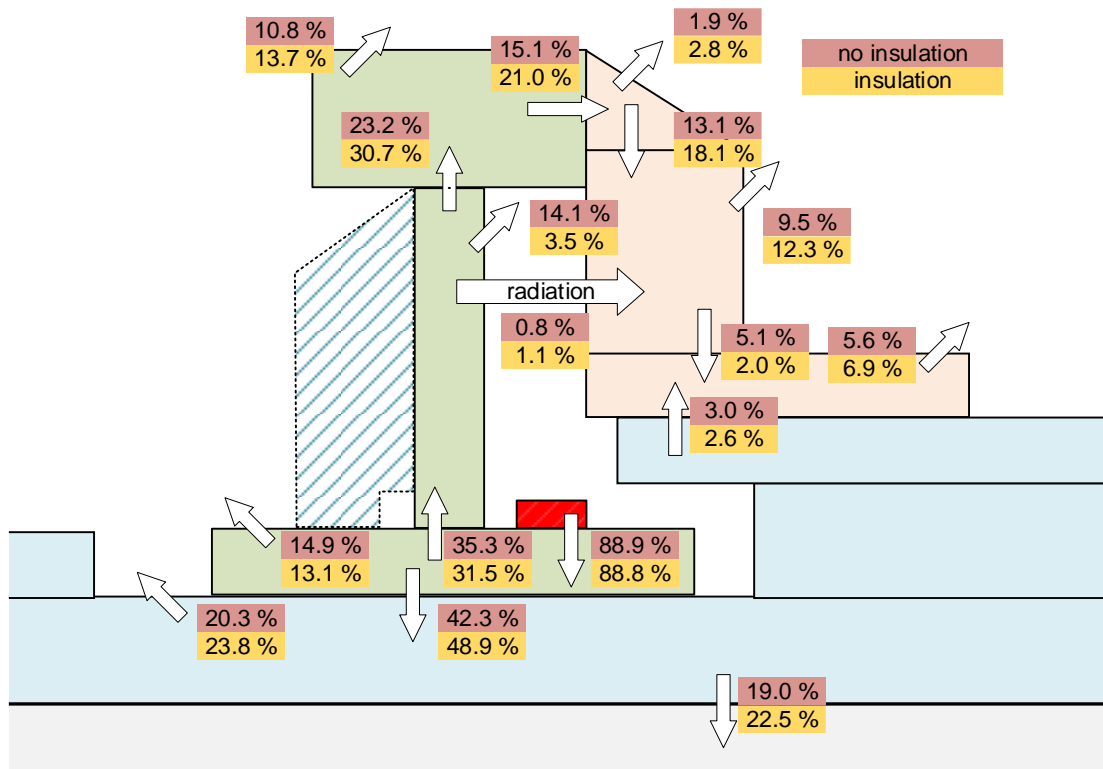
Figure 36: percentage of heat flows to total thermal power at ϑ_u = -10 °C; P = 300 W/m; 15 km / h wind; no precipitation; on Y-side with and without stock rail insulation (straight arrows indicate heat transfer between components; diagonal arrows indicate heat dissipation)

At a wind speed of 15 km / h, almost as much heat is fed into the foot of the stock rail as in windless conditions (**Figure 36**). This is because the calculation model takes into account a lower wind speed in the space between the stock rail and the tongue rail due to the protected position. The gap is larger on the X-side and clearly open at the top so that the same wind speed is assumed in the gap as on the outer sides. Due to forced convection, the surfaces of the components emit more heat to the environment. As a result, the heat flows also change qualitatively. In this case, the foot of the tongue rail is a heat sink of the components. Compared to the X-side, the heat flows between stock rail with and without insulation are more different here.

9.3   Conclusion of the analysis of the heat flows

The analysis of the heat flows shows that in almost all cases only a very small part of the heat provided by the heating rod reaches the tongue rail. Insulating the web of the stock rail significantly reduces the heat dissipation of the web. However, the thermal influence of the insulation is reduced the further away from it. This is because heat dissipation in adjacent subcomponents is greater with existing stock rail insulation. Already the analysis of the calculation scenarios showed that the insulation improves the temperature distribution only insignificantly. The reason for this is that the surface covered by the

insulation is relatively small compared to the total surface of the point components. A possible solution would be to install insulation on additional surfaces, if this does not restrict the operation and setting of the point (e.g. inside web of stock rail or tongue rail).

The calculations without the influence of wind show a large amount of heat being conducted from the base plate into the sleeper. The heat in the sleeper is dissipated into the track bed and is therefore no longer available for heating the tongue rail and slide chair. From a thermal point of view, however, the aim is to achieve the lowest possible heat transfer into the sleeper. In the heat network model, a plastic mat between the base plate and sleeper is already taken into account. An increase in the thickness of this mat increases the thermal resistance and thus reduces the heat conduction to the sleeper. Supplementary investigations showed, however, that the heat flow into the tongue rail is only slightly increased.

10 Conclusion and outlook

In the EuroPoint project, a common model of a point was defined taking into account the interests of all project partners. The components were constructed as thermal network models and these were again verified experimentally. The separate heating networks were linked and the whole model was verified under laboratory and outdoor conditions. Special attention was paid to the implementation of the environmental conditions for the real application case under different weather conditions. The complete point model is able to calculate static and dynamic heating processes and to output temperatures and heat flows in high resolution.

The heating calculations showed that no heat flow occurs between both sides of the point. Therefore, both sides of the point can be considered separately. The thermally more critical case occurs on the point side where stock rail and tongue rail do not touch each other. The calculations of different application scenarios of the railway companies showed that for no examined case where wind or precipitation occurred, a faultless operation of the point could be guaranteed. This is due to the low temperatures at the tongue rail and on the slide chair. Even insulation of the web of the stock rail does not significantly improve the temperature distribution. An analysis of the heat flows confirmed the low effect of stock rail insulation and showed that a large part of the generated heat is dissipated from the base plate into the sleeper.

The completely verified heat network of the point can be used in the future as a basic tool for calculation for optimization approaches. The major part of the effort lies in the design of the thermal network. Further adjustments or modifications can usually be implemented quite easily. Therefore, it is of clear advantage to continue using the thermal network of the point in order to improve the point thermally further.

As only a low heat transfer from stock rail to tongue rail could be determined, possibilities should be considered where the heat is fed directly into the tongue rail. An additional

heating element mounted on the web of the tongue rail would be conceivable, for example.

The total energy requirement of electric point heaters is not an insignificant factor for a railway company. In order to save costs, the most efficient operation is therefore to be aimed at. One possibility would be an intelligent control of the point heater, which, depending on the ambient conditions, not only switches the point heater on and off but also adjusts its performance. In this way, much more powerful point heating systems could be installed. On the one hand, the control system would make it possible to intercept thermally critical situations and, on the other hand, to keep the heating power requirement low during normal operation.

11 Literatur

[1] Böhme, H. A.: Mittelspannungstechnik - Schaltanlagen berechnen und entwerfen. 2. stark bearb. Aufl. Berlin, Paris, London: HUSS-MEDIEN GmbH Verlag Technik 2005. ISBN 3-341-01495-0.

[2] Verein Deutscher Ingenieure: VDI Wärmeatlas – Berechnungsblätter für den Wärmeübergang. 8. überarb. und erw. Auflage Berlin, Heidelberg, u.a.: Springer 1997. ISBN 3-540-62719-7.

[3] Adam R.; Schladitz M; Döring N.: 3. Zwischenbericht Europoint HH 01/15

[4] Schladitz M, Adam R: 4. Zwischenbericht Europoint HH 01/15

[5] Schladitz M, Adam R: 5. Zwischenbericht Europoint HH 01/15

[6] Baehr, H.; Stephan, K.: Wärme- und Stoffübertragung. 2. Auflage; Springer-Verlag Berlin

[7] http://scienceblogs.de/frischer-wind/2009/10/12/wie-berechnet-man-die-hohenabhangige-windgeschwindigkeit/ (Stand: 11.07.19)

[8] Kleemann, M.; Meliß, M.: Regenerative Energiequellen, 2. Auflage: Springer-Verlag 1993

[9] Berg, I: Untersuchungen zur Strombelastbarkeit der Geräte der Elektroenergieübertragung unter Freiluftatmosphäre

[10] Kasten, F.: Strahlungsaustausch zwischen Oberflächen und Atmosphäre, VDI-Berichte Nr. 721, VDI Verlag, 1989

[11] Schladitz M, Adam R;: 6. Zwischenbericht Europoint HH 01/15

Attachments

Attachment 1:   quantities for heating calculation

thermal quantity	symbol	unit
temperature	ϑ	°C
temperature difference	$\Delta\vartheta$	K
temperature rise	Q	K
heat flow; thermal power	P, $\dot{Q}$	W
heat flux	$\dot{q}$	W m^{-2}
thermal conductivity	λ	W m^{-1} K^{-1}
thermal capacity	C_{th}	W s K^{-1}
specific thermal capacity	c_p	W s kg^{-1} K^{-1}
thermal energy	Q	W s
heat transfer coefficient	α	W m^{-2} K^{-1}
reference length	l_w	m
surface for heat emission	O	m^2
Emissionsgrad einer Oberfläche	ε_1	-
resulting emissivity between two surfaces	ε_{12}	-
thermal resistor	R_{th} or R	K W^{-1}
	th	thermal
	l	conduction
index	K	convection
	S	radiation
	1; 2	number of the component

Attachment 2: parameter list for stock rail and heating rod

parameter name	value	unit	meaning
conductivity_steal	45	W (m K)$^{-1}$	thermal conductivity rail material
conductivity_rod	15	W (m K)$^{-1}$	thermal conductivity heating rod
eps_stock	0.835		emissivity stock rail
eps_rod	0.23		emissivity heating rod
foot_width	0.15	m	width section foot
foot_height	0.0169	m	height foot
foot_width_1	0.0645	m	width section foot
foot_width_2	0.021	m	width section foot
foot_width_3	0.0125	m	width section foot
rod_width	0.013	m	width heating rod
rod_height	0.0055	m	height heating rod
web_height	0.1176	m	height web
web_width	0.021	m	width web
head_width	0.072	m	width section head
head_width_1	0.0255	m	width section head
head_width_2	0.021	m	width section head
head_height	0.0375	m	height head
foot_width_4	0.039	m	width section foot
entire_height	0.172	m	total height
c_1_stock	0.2		similarity parameter
n_1_stock	0.25		similarity parameter

Attachment 3:   excerpt from the technical drawing of the tongue rail

Attachment 4:   parameter list for the tongue rail

parameter name	value	unit	meaning
length_A	0.25/2	m	length subsection
length_B	0.88/3	m	length subsection
length_C	1.4/4	m	length subsection
length_D	1.309/4	m	length subsection
width_A_1	0.018	m	width
width_A_2	0.026	m	width
width_A_3	0.076	m	width
width_A_11	0.0045	m	width head
height_A_1	0.027	m	width head
height_A_2	0.058	m	height web
height_A_3	0.023	m	height foot
eps_tongue	0.835		emissivity
l_ref_A	0.108	m	reference length
l_triangle_A	0.02846	m	length edge head
lamda_rail	45	W (m K)$^{-1}$	thermal conductivity
c_tongue	0.2		similarity parameter
n_tongue	0.25		similarity parameter
rad_trA_head	0.057*length_A*global_rad	W	incident radiation
rad_trA_web	0.142*length_A*global_rad	W	incident radiation
rad_trA_foot	0.122*length_A*global_rad	W	incident radiation
rain_f_par	0.1		rain proportion tongue rail
rain_tongue	5		rain proportion tongue rail
width_B_1	0.022	m	width
width_B_2	0.022	m	width
width_B_3	0.076	m	width
width_B_11	0.0055	m	width head

height_B_1	0.030		width head
height_B_2	0.058		height web
height_B_3	0.023		height foot
l_ref_B	0.111	m	reference length
l_triangle_B	0.03195	m	length edge head
rad_trB_head	0.064*length_B*global_rad		incident radiation
rad_trB_web	0.138*length_B*global_rad		incident radiation
rad_trB_foot	0.122*length_B*global_rad		incident radiation
width_C_1	0.023	m	width
width_C_2	0.021	m	width
width_C_3	0.076	m	width
width_C_11	0.00575	m	width head
height_C_1	0.037	m	height head
height_C_2	0.058	m	height web
height_C_3	0.023	m	height foot
l_ref_C	0.118	m	reference length
l_triangle_C	0.03875	m	length edge head
rad_trC_head	0.077*length_C*global_rad		incident radiation
rad_trC_web	0.137*length_C*global_rad		incident radiation
rad_trC_foot	0.122*length_C*global_rad		incident radiation
width_D_1	0.030	m	width
width_D_2	0.014	m	width
width_D_3	0.076	m	width
width_D_11	0.00525	m	width head
height_D_1	0.043	m	height head
height_D_2	0.058	m	height web
height_D_3	0.023	m	height foot
l_ref_D	0.124	m	reference length
l_triangle_D	0.04426	m	length edge head

rad_trD_head	0.0975*length_D*global_rad		incident radiation
rad_trD_web	0.130*length_D*global_rad		incident radiation
rad_trD_foot	0.122*length_D*global_rad		incident radiation
trapezoid_D	0.009	m	width section head

Attachment 5: technical drawing of base plate and slide chair
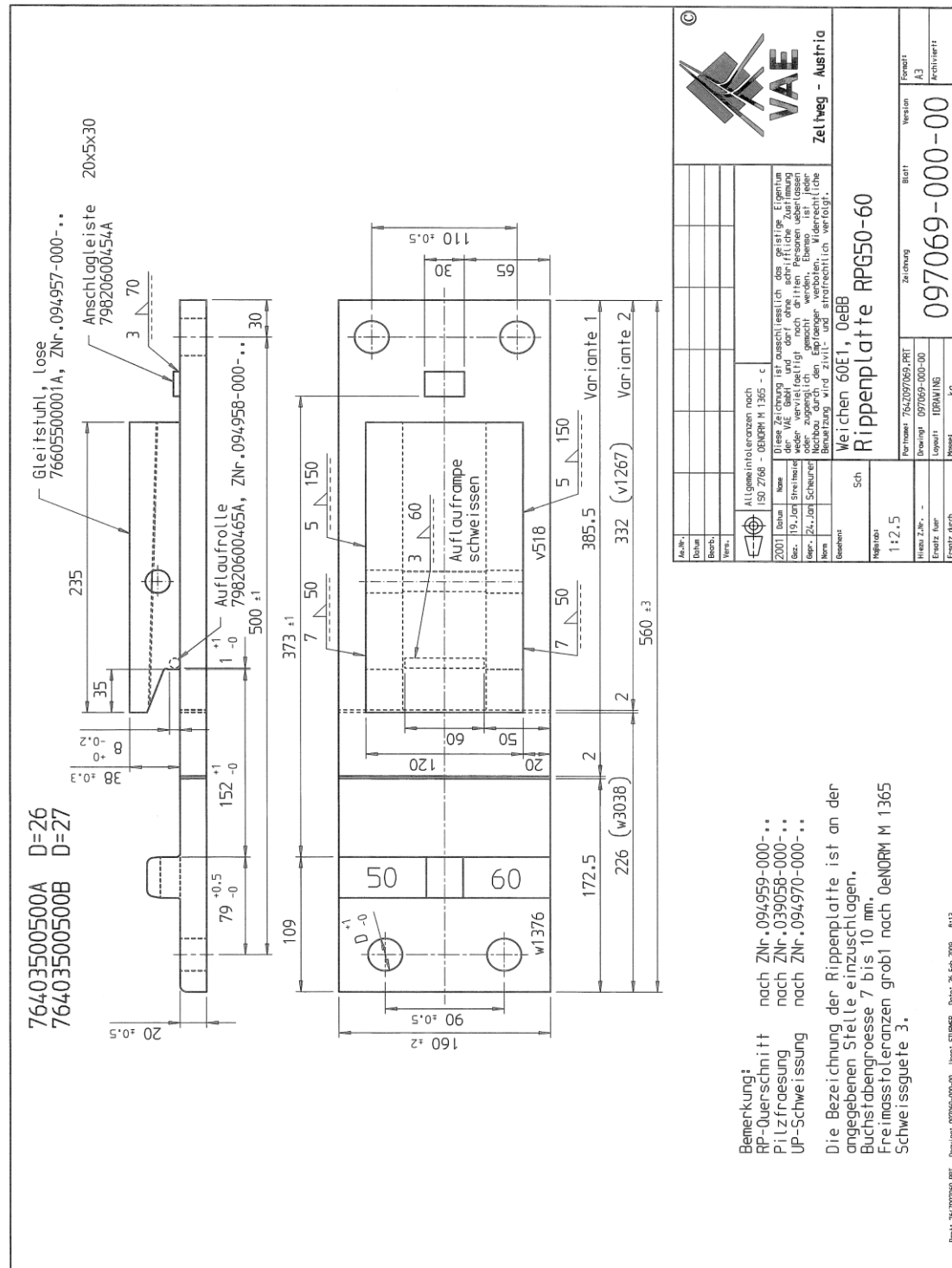
Attachment 6:   parameter list for base plate and slide chair

parameter name	value	unit	meaning
thermal_conductivity	52	W (m K)$^{-1}$	thermal conductivity
eps_assembly	0.89		emissivity
c1_assembly	0.555		similarity parameter
n1_assembly	0.25		similarity parameter
characteristic_length	0.56	m	reference length
assembly_width_1	0.02	m	width section
assembly_width_2	0.0285	m	width section
assembly_width_3	0.063	m	width section
assembly_width_1_half	0.01	m	width section
assembly_width_2_half	0.01425	m	width section
assembly_width_3_half	0.0315	m	width section
rip_plate_length_1	0.076	m	length section
rip_plate_length_2	0.033	m	length section
rip_plate_length_3	0.117	m	length section
rip_plate_length_4_1	0.0225	m	length section
rip_plate_length_4_2	0.12	m	length section
rip_plate_length_4_3	0.0575	m	length section
slide_chair_high_1	0.019	m	height slide chair
slide_chair_high_2	0.019	m	height slide chair
rip_plate_length_5	0.099	m	length section
slide_chair_length_1	0.0225	m	length section
slide_chair_length_2	0.12	m	length section
slide_chair_length_3	0.0575	m	length section
rip_plate_high	0.02	m	height section
rip_plate_high_2	0.038	m	height section
rip_plate_length_4	0.035	m	length section
slide_chair_length_0	0.035	m	length section

Attachment 7:   parameter list for the sleeper

parameter name	value	unit	meaning
laenge	2.6	m	length sleeper
hoehe	0.22	m	height sleeper
breite	0.18	m	width sleeper
H	0.22	m	height sleeper
B	0.3	m	width sleeper
nx	13		subdivision length
ny	4		subdivision width
nz	1		subdivision height
lambda	2.3	W (m K)$^{-1}$	thermal conductivity
temp_zero	theta_amb	°C	ambient temperature
konvc1	0.15		similarity parameter
dichte_beton	2600		density
charlen	0.0605		reference length
konvn1	0.33		similarity parameter
eps1	0.94		emissivity
breitev	0.055	m	width section
lambda_h_vh	2.94	m	separate thermal conductivity
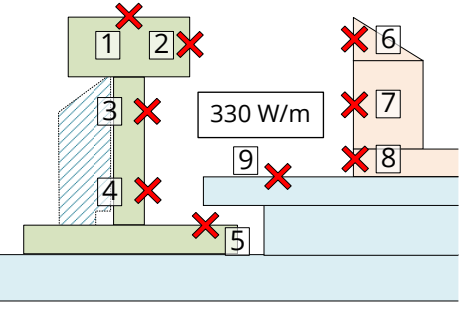
lengths in cm
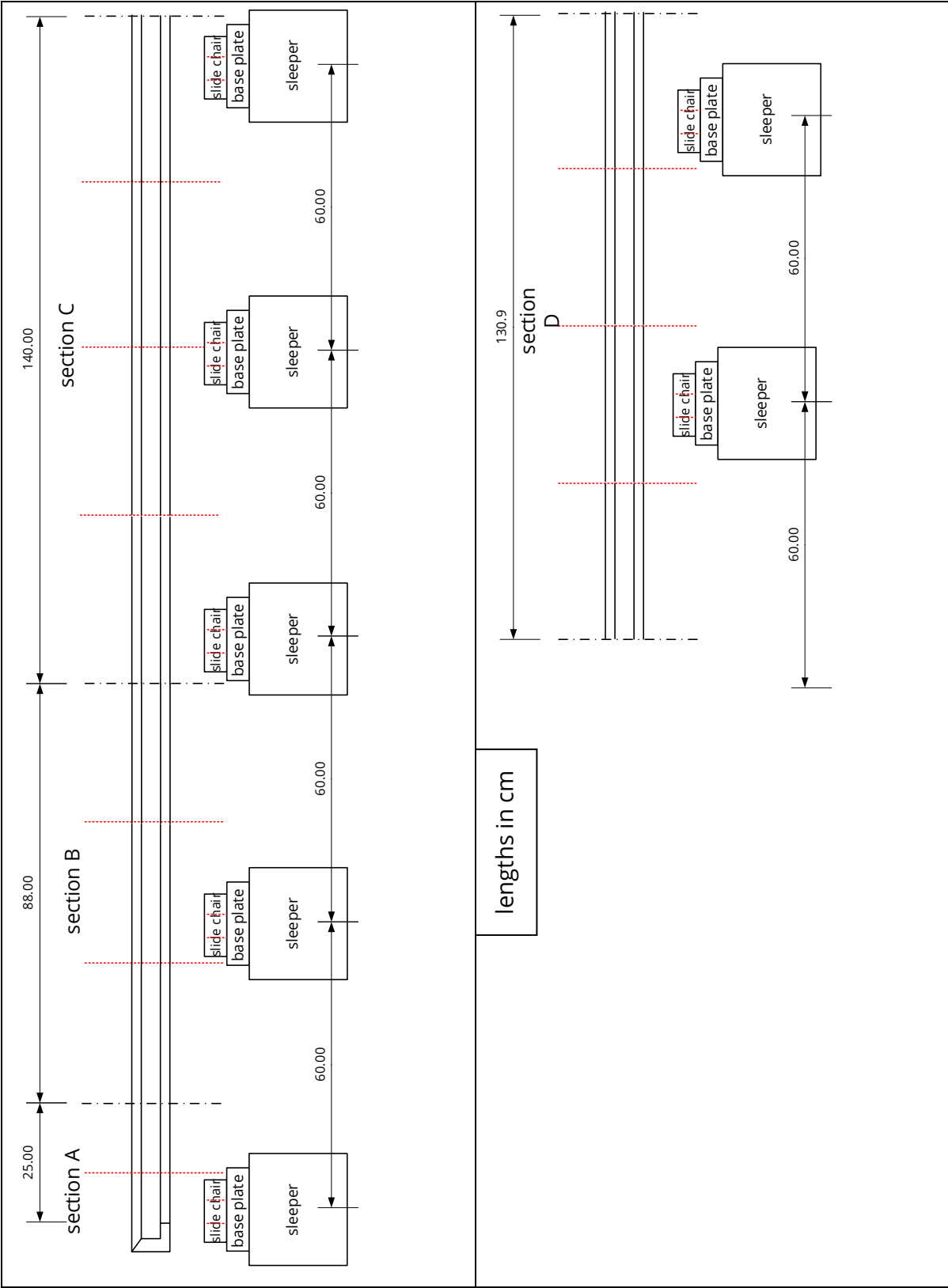
Attachment 9: allocation of the components to the respective libraries in the TNM model
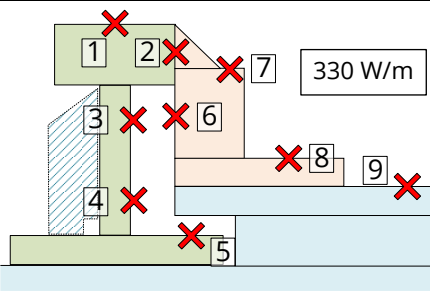
component	library	name
stock rail	stock_rail_hierch	Stock_Rail_A etc.
tongue rail	tongue_rail_a_hierch etc.	A_section etc.
base plate and slide chair	base_plate_slide_chair	slide_chair_base_plate_hierch
sleeper	sleeper	sleeper_half

Attachment 10: calculated temperatures of the X-side of the point for ÖBB scenarios (scenarios with stock rail insulation in bold)

	position								
	1	2	3	4	5	6	7	8	9
	ϑ_1 in °C	ϑ_2 in °C	ϑ_3 in °C	ϑ_4 in °C	ϑ_5 in °C	ϑ_6 in °C	ϑ_7 in °C	ϑ_8 in °C	ϑ_9 in °C
ÖBB 1: 0 °C; 24 km/h; 30 cm / 12 h	1.8	2.0	4.1	7.0	12.7	0.0	0.0	0.0	0.9
ÖBB 2: 0 °C; 30 km/h; 40 cm / 12 h	0.9	1.0	2.8	5.4	10.4	0.0	0.0	0.0	0.6
ÖBB 3: 0 °C; 30 km/h; 30 cm / 12 h	1.5	1.6	3.4	6.1	11.4	0.0	0.0	0.0	0.8
ÖBB 4: 0 °C; 30 km/h; 50 cm / 12 h	0.4	0.6	2.3	4.8	9.4	0.0	0.0	0.0	0.4
ÖBB 5: -5 °C; 50 km/h; 10 cm / 12 h	-2.6	-2.6	-1.3	1.0	6.1	-4.6	-4.5	-4.6	-3.1
ÖBB 6: -5 °C; 10 km/h; 50 cm / 12 h	0.2	0.3	2.6	5.8	12.0	-5.0	-5.0	-5.0	-2.4
ÖBB 7: -5 °C; 10 km/h; 50 cm / 12 h	0.8	0.9	3.6	7.1	12.8	-5.0	-5.0	-5.0	-1.9
ÖBB 8: -5 °C; 24 km/h; 10 cm / 12 h	0.5	0.5	2.2	5.2	11.6	-4.3	-4.3	-4.3	-1.1
ÖBB 9: -5 °C; 24 km/h; 10 cm / 12 h	1.8	1.8	4.0	7.2	13.1	-4.3	-4.2	-4.2	-0.7
ÖBB 10: -10 °C; 24 km/h; 10 cm / 12 h	-3.3	-3.3	-1.7	1.3	8.0	-8.0	-7.9	-7.9	-5.3
ÖBB 11: -10 °C; 24 km/h; 10 cm / 12 h	-1.2	-1.2	0.9	4.0	10.1	-7.9	-7.8	-7.7	-4.7

Attachment 11: calculated temperatures of the Y-side of the point for ÖBB scenarios (scenarios with stock rail insulation in bold)
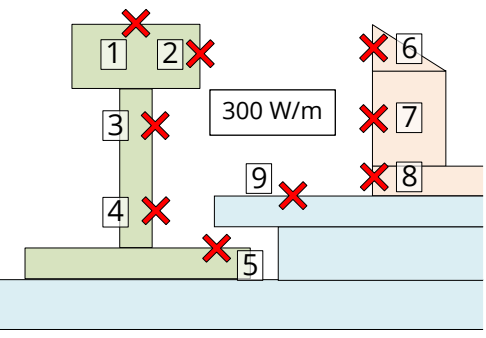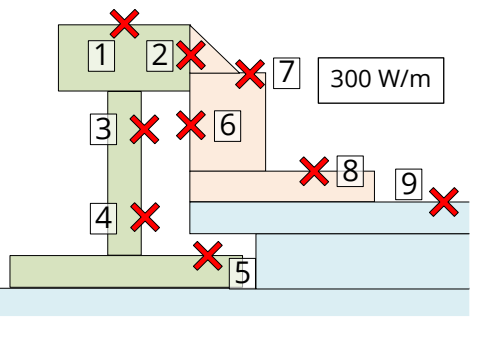

	position								
	1	2	3	4	5	6	7	8	9
	ϑ_1 in °C	ϑ_2 in °C	ϑ_3 in °C	ϑ_4 in °C	ϑ_5 in °C	ϑ_6 in °C	ϑ_7 in °C	ϑ_8 in °C	ϑ_9 in °C
ÖBB 1: 0 °C; 24 km/h; 30 cm / 12 h	3.2	2.6	7.9	13.7	24.4	1.3	0.9	0.6	2.7
ÖBB 2: 0 °C; 30 km/h; 40 cm / 12 h	2.3	1.9	6.8	12.2	22.8	0.8	0.4	0.2	2.0
ÖBB 3: 0 °C; 30 km/h; 30 cm / 12 h	2.9	2.4	7.4	12.9	23.5	1.1	0.8	0.5	2.5
ÖBB 4: 0 °C; 30 km/h; 50 cm / 12 h	1.8	1.5	6.3	11.6	22.2	0.5	0.1	0.0	1.7
ÖBB 5: -5 °C; 50 km/h; 10 cm / 12 h	-0.5	-1.0	2.6	7.1	16.8	-1.9	-2.0	-2.4	-1.1
ÖBB 6: -5 °C; 10 km/h; 50 cm / 12 h	1.3	1.0	5.9	11.3	22.0	-0.1	-0.3	-1.2	-0.5
ÖBB 7: -5 °C; 10 km/h; 50 cm / 12 h	2.3	1.8	7.8	13.9	24.3	0.4	0.1	-0.3	1.0
ÖBB 8: -5 °C; 24 km/h; 10 cm / 12 h	2.2	1.6	6.0	11.2	21.4	0.5	0.3	-0.1	1.0
ÖBB 9: -5 °C; 24 km/h; 10 cm / 12 h	4.8	3.9	10.2	16.2	26.1	2.0	1.8	1.0	2.4
ÖBB 10: -10 °C; 24 km/h; 10 cm / 12 h	1.2	0.4	5.0	10.3	20.5	-1.0	-1.1	-1.9	-1.5
ÖBB 11: -10 °C; 24 km/h; 10 cm / 12 h	4.4	3.3	9.5	15.3	24.6	1.3	1.2	0.0	0.6
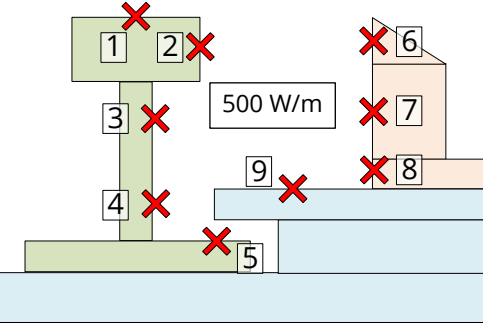
Attachment 12: calculated temperatures of the X-side of the point for SBB scenarios

	position								
	1	2	3	4	5	6	7	8	9
	ϑ_1 in °C	ϑ_2 in °C	ϑ_3 in °C	ϑ_4 in °C	ϑ_5 in °C	ϑ_6 in °C	ϑ_7 in °C	ϑ_8 in °C	ϑ_9 in °C
SBB 1: 0 °C; 0 km/h; no snow	32.9	33	34.5	37.6	44.7	7.9	8.0	8.3	16.4
SBB 2: 0 °C; 0 km/h; heavy rain	5.8	6.1	10.1	14.8	22.4	0.2	0.2	0.3	2.6
SBB 3: 0 °C; 0 km/h; 30 cm / 12 h	6.9	7.2	11.1	16.0	23.6	0.0	0.0	0.0	2.5
SBB 4: 0 °C; 15 km/h; 30 cm / 12 h	2.4	2.6	4.8	8.0	13.8	0.0	0.0	0.0	1.1
SBB 5: 0 °C; 30 km/h; 30 cm / 12 h	1.2	1.3	3.0	5.5	10.3	0.0	0.0	0.0	0.6
SBB 6: -5 °C; 0 km/h; kein Schnee	28.9	28.9	30.4	33.5	40.5	3.8	3.8	4.1	12.0
SBB 7: -5 °C; 0 km/h; 30 cm / 12 h	5.7	6.0	9.6	14.1	21.6	-4.9	-4.9	-4.6	1.6
SBB 8: -5 °C; 15 km/h; 30 cm / 12 h	0.1	0.2	2.0	4.9	10.6	-5.0	-5.0	-5.0	-2.1
SBB 9: -5 °C; 30 km/h; 30 cm / 12 h	-2.4	-2.4	-0.9	1.6	6.7	-5.0	-5.0	-5.0	-3.8
SBB 10: -10 °C; 0 km/h; kein Schnee	24.8	24.8	26.3	29.3	36.3	-0.5	-0.4	-0.1	7.5
SBB 11: -10 °C; 0 km/h; 30 cm / 12 h	4.5	4.7	8.1	12.4	19.7	-9.2	-9.2	-8.8	2.4
SBB 12: -10 °C; 15 km/h; 30 cm / 12 h	-4.1	-4.0	-2.1	0.8	6.9	-10.0	-10.0	-10.0	-7.0
SBB 13: -10 °C; 30 km/h; 30 cm / 12 h	-7.4	-7.4	-5.8	-3.3	1.8	-10.0	-10.0	-10.0	-8.7
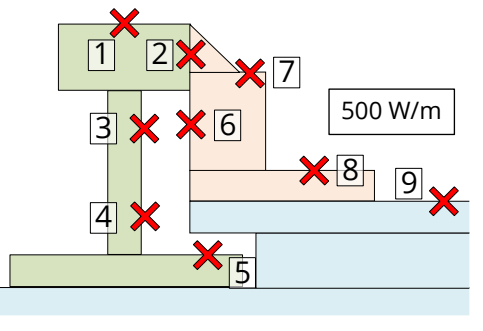
Attachment 13: calculated temperatures of the Y-side of the point for SBB scenarios

	position								
	1	2	3	4	5	6	7	8	9
	ϑ_1 in °C	ϑ_2 in °C	ϑ_3 in °C	ϑ_4 in °C	ϑ_5 in °C	ϑ_6 in °C	ϑ_7 in °C	ϑ_8 in °C	ϑ_9 in °C
SBB 1: 0 °C; 0 km/h; no snow	25.9	24.8	29.7	34.4	42.6	22.6	22.6	21.0	17
SBB 2: 0 °C; 0 km/h; heavy rain	4.4	3.7	10.1	16.3	26.5	2.0	1.6	1.2	3.9
SBB 3: 0 °C; 0 km/h; 30 cm / 12 h	4.8	4.0	10.5	16.7	26.9	2.1	1.7	1.1	4.0
SBB 4: 0 °C; 15 km/h; 30 cm / 12 h	3.3	2.7	8.0	13.6	23.5	1.4	1.0	0.6	2.8
SBB 5: 0 °C; 30 km/h; 30 cm / 12 h	2.5	2.1	6.7	11.7	21.36	1.0	0.7	0.4	2.2
SBB 6: -5 °C; 0 km/h; kein Schnee	21.8	20.7	25.6	30.3	38.4	18.5	18.5	16.9	12.7
SBB 7: -5 °C; 0 km/h; 30 cm / 12 h	3.9	3.2	9.2	15.1	24.9	1.6	1.2	0.6	2.2
SBB 8: -5 °C; 15 km/h; 30 cm / 12 h	1.4	1.0	5.3	10.2	19.7	0.0	-0.1	-0.9	0.4
SBB 9: -5 °C; 30 km/h; 30 cm / 12 h	-0.6	-1.1	2.9	7.5	16.8	-2.2	-2.4	-2.9	-1.4
SBB 10: -10 °C; 0 km/h; kein Schnee	17.7	16.6	21.5	26.4	34.2	14.5	14.5	12.8	8.3
SBB 11: -10 °C; 0 km/h; 30 cm / 12 h	3.1	2.5	7.9	13.5	22.9	1.0	0.7	0.1	0.7
SBB 12: -10 °C; 15 km/h; 30 cm / 12 h	-2.3	-3.0	1.6	6.6	16.1	-4.4	-4.6	-5.4	-4.1
SBB 13: -10 °C; 30 km/h; 30 cm / 12 h	-5.2	-5.6	-1.7	2.8	12.1	-6.6	-6.9	-7.4	-6.2

Attachment 14: calculated temperatures of the X-side of the point for ProRail scenarios

	Position								
	1	2	3	4	5	6	7	8	9
	ϑ_1 in °C	ϑ_2 in °C	ϑ_3 in °C	ϑ_4 in °C	ϑ_5 in °C	ϑ_6 in °C	ϑ_7 in °C	ϑ_8 in °C	ϑ_9 in °C
ProRail 1: 0 °C; 19.4 km/h; 1 cm/h	7.1	7.2	10.6	15.7	26	0	0.1	0.2	2.4
ProRail 2: -5 °C; 28.4 km/h; -	3.6	3.5	5.9	10.3	20.1	-3.5	-3.4	-3.3	1
ProRail 3: -10 °C; 38.5 km/h; -	-3.7	-3.8	-1.7	2.3	11.2	-8.2	-8.1	-8	-5.2
ProRail 4: -10 °C; 38.5 km/h; 1 cm/h	-4.6	-4.6	-2.4	1.5	10.2	-8.9	-8.8	-8.8	-5.9

Attachment 15: calculated temperatures of the Y-side of the point for ProRail scenarios

	Position								
	1	2	3	4	5	6	7	8	9
	ϑ_1 in °C	ϑ_2 in °C	ϑ_3 in °C	ϑ_4 in °C	ϑ_5 in °C	ϑ_6 in °C	ϑ_7 in °C	ϑ_8 in °C	ϑ_9 in °C
ProRail 1: 0 °C; 19.4 km/h; 1 cm/h	8.8	7.5	16.1	25	41.1	4.9	4.4	3.5	7.2
ProRail 2: -5 °C; 28.4 km/h; -	9.3	8.1	15	22.8	38.1	5.9	5.9	4.9	6.4
ProRail 3: -10 °C; 38.5 km/h; -	2.1	1.1	7.5	14.9	30.1	-0.7	-0.8	-1.6	0.2
ProRail 4: -10 °C; 38.5 km/h; 1 cm/h	-1.2	-2.0	3.8	10.9	25.9	-3.5	-3.7	-4.2	-2.6